ASTRONOMY & ASTROPHYSICS
SUPPLEMENT SERIES

Astron. Astrophys. Suppl. Ser. **67**, 395-422 (1987)

0.6 GHz mapping of extended radio galaxies. I. Edge-brightened double sources

W. J. Jägers

Sterrewacht Leiden, P.O. Box 9513, 2300 RA Leiden, The Netherlands

Received November 20, 1985 ; accepted May 14, 1986

Summary. — Radio observations made with the Westerbork telescope at 0.6 GHz are presented for 9 edge-brightened double sources : 3C33.1, 3C35, 3C111, B0844+316, 3C223, 4C26.35A, 4C74.17.1, 3C390.3 and 3C452. Previously observed Westerbork data at 1.4 GHz are convolved for comparison with the 0.6 GHz observational data. Beside maps of the total intensity and linear polarization structure, the distibutions of the spectral index, the depolarization and the rotation of the polarization position angle between 0.6 GHz and 1.4 GHz have been derived. Integrated values for the total intensity and the polarization are also given.

Key words : radio sources — total intensity — linear polarization.

1. Introduction.

Measurements of the radio structure have contributed considerably to the knowledge of the production and evolution of extragalactic radio sources. In particular, multifrequency measurements of intensity and polarization distributions allow useful constraints to be placed on thermal plasma and magnetic field configurations within the sources and give meaningful information about the energy loss processes (e.g. Van Breugel, 1980 ; Willis *et al.*, 1981).

In recent years, the emphasis of such studies has been more and more on exploring the small scale structures such as jets, cores, and hot spots, with high resolution techniques at frequencies of 1.4 GHz and above. In multifrequency comparisons it is clearly important to extend the wavelength coverage over as wide a wavelength range as possible. However, in most cases the lower frequency observations carried out until now provided only a few pixels over a typical radio source. This lack of detail at low frequencies was one of the limitations affecting the multifrequency comparison. The fourfold increase in pixel density provided by the « new » 3 km Westerbork Synthesis Radio Telescope (WSRT) and the improved properties of the system (the system noise temperature is now about 100 K at 0.6 GHz instead of 350 K in the old system) at frequencies below 1.4 Ghz have prompted the initiation of a program to systematically map strong extended radio sources with the WSRT at 0.6 GHz. The main purpose of this program is to make comparisons between 0.6 GHz (3 km) and 1.4 GHz (1.5 km) WSRT data and to interpret the resulting information on magnetic fields, thermal plasma distributions and energy loss mechanisms within the context of current models of radio sources.

Our sample is limited to radio sources larger than 200 arcsec and those with declinations above 25°. This gives at least 9 pixels across a source at 0.6 GHz and a synthesized beam whose ellipticity does not exceed 2.5. We attempted to include all sources known to satisfy these conditions in 1980 when the project began. The resulting sample comprises 30 radio sources, 16 of which are 3C-sources. The sample is representative of the various morphological types found among radio galaxies (e.g. Miley, 1980).

This paper is the first of a series describing the 0.6 GHz observations of the sample, and a comparison with observations made at 1.4 GHz. This paper deals with 9 sources which (adopting the classification scheme of Miley, 1980) have narrow edge-brightened double morphologies. These Cygnus A-type sources are 0104+321 (3C33.1), 0106+492 (3C35), 0415+379 (3C111), 0844+316 (B2), 0936+361 (3C223), 1155+266 (4C26.35A), 1209+745 (4C74.17.1), 1845+797 (3C390.3) and 2243+394 (3C452). Presentation of the results for the spatial distributions of several quantities inevitably requires considerable space. We therefore present these results here. A general discussion of the results and their interpretation will be given in a subsequent paper.

2. Observations and data reduction.

2.1 THE 0.6 GHz OBSERVATIONS. — Each of the 9 radio sources was observed for 12 hours with the 3 km WSRT at a frequency of 608.5 MHz and a bandwidth of 2.5 MHz. The WSRT and its data reduction system have been described in detail by Baars and Hooghoudt (1974), Högbom and Brouw (1974) and Van Someren Grève (1974). The parameters of these 0.6 GHz observations are listed in table I.

Column 1 : the source name.

Column 2 : an alternative source name.

Column 3, 4 : the centre of the observed field in equatorial coordinates (1950.0).

The diameter of the primary beam (FWHM) at 0.6 GHz is 1.4 degrees.

Column 5, 6 : the centre of the observed field in galactic coordinates.

Column 7 : the date of observation. Each source was observed for 12 hours.

Column 8 : the receivers used. The sensitivity of the receivers was improved at the end of 1981.

The « old » receivers had a system noise temperature of about 350 K compared with a system noise temperature of about 100 K for the « new » receivers.

Column 9 : the half power width of the synthesized beam. The observations have been done with 40 interferometers having baselines ranging from 72 m to 2736 m in increments of 72 m. A Gaussian taper was applied to the visibility data reaching 25 % at 2736 m.

Column 10, 11 : the R.M.S. noise and the confusion level in the total intensity map (to be discussed below).

Using standard calibrators (Tab. II) the usual corrections to the amplitudes and phases of the visibilities were applied to compensate for drifts in the gain and phase stability of the receivers (WSRT Users Manual, 1980). The uncertainties in the phases due to incorrect baseline determination is negligible at this low frequency as is the effect of atmospheric disturbances. However, the ionosphere is a potent source of disturbances (Spoelstra, 1983). Spoelstra showed that the correction for a combination of both horizontal and vertical gradients in the electron density distribution in the ionosphere can improve the observations considerably, especially at 0.6 GHz. Variations of ionospheric refraction on small time scales (< few hours) are still present in the data due to a insufficient number of measurements in the ionosphere. In particular, it is not possible to derive reliable corrections around sunrise, when rapid changes in the vertical electron density occur. These insufficient corrections show up in the maps in the form of « spokes » around point components. This can clearly be seen in the total intensity maps of the radio sources 3C111 and 3C452.

The corrected observations were than Fourier transformed to obtain maps at the four Stokes parameters I, Q, U and V. I is the total intensity of the radio emission, Q and U determine the linear polarization and V the circular polarization. The (dirty) I, Q and U maps were cleaned using the « clean » technique developed by Högbom (1974) to remove the effects of grating rings and near-in side lobes and to correct for the distortions introduced by missing short spacings. After restoration, the cleaned maps were corrected for primary beam attenuation.

2.2 THE 1.4 GHz OBSERVATIONS. — One of the aims of observing the radio sources at 0.6 GHz was to compare with existing 1.4 GHz data. For 8 of the 9 sources 1.4 GHz observations made with the 1.5 km WSRT were available but there are none for the source 1155+266 (4C26.35A). The 1.4 GHz observations were re-reduced using as similar as possible procedures as for the 0.6 GHz observations. To obtain a satisfactory comparison between maps at two different frequencies, similar resolution must be produced. To achieve this, the visibility data must be used from baselines as closely as possible the same length in units of wavelengths (λ). The data at 0.6 GHz was tapered with a Gaussian which falls to 0.25 at the longest baseline ($2736\ \mathrm{m} \simeq 5553\ \lambda$). At 1.4 GHz the same taper was used with the weight of 0.25 being applied to the baseline $2736 \times 608.5/\upsilon$ m, were υ is the exact frequency of the observation in MHz. Where certain baselines were missing, the corresponding ones at the other frequency were also omitted, especially where the shortest baselines were involved. The shortest baseline at 0.6 GHz (72 m) corresponds to 31 m at 1.4 GHz. All the 1.4 GHz observations were made with a shortest spacing of either 36 m or 54 m except for B0844+316 where it was 72 m. For the comparison the 0.6 GHz observations of B0844+316 were reduced again excluding the 72 m spacing. Relevant parameters of the 1.4 GHz observations are listed in table III.

Column 1 : the source name.

Column 2 : an alternative source name.

Column 3, 4 : the exact frequency and bandwidth of the 1.4 GHz observation.

Column 5 : the date of observation.

Column 6, 7 : the R.M.S. noise and confusion level in the total intensity maps, determined from the convolved maps.

Column 8 : notes on the references corresponding to the 1.4 GHz full resolution maps. See the notes to table III.

3C111 was reobserved in 1977. Older observations were published by Högbom and Carlsson in 1974.

From the *UV* plane the Fourier transform was made to obtain the I, Q, U and V-maps. The 1.4 GHz dirty maps were then further reduced as the 0.6 GHz maps had been. The maps were restored, after cleaning, with a similar Gaussian beam. As the observing centres of the maps at the two frequencies were usually different, the 1.4 GHz maps were shifted and regridded to the maps at 0.6 GHz. The intensity of the linear polarization P is defined as $\left(Q^2 + U^2\right)^{1/2}$, and the position angle of the electric vector ϕ is $1/2 \arctan U/Q$. The percentage of polarization, $\% P$, is the fraction of the total intensity that is linearly polarized. From the various maps at the two frequencies the distributions of the spectral index α (the flux $F_\upsilon\ \alpha\ \upsilon^{-\alpha}$), the depolarization DP $\left(= \% P_{0.6\,\mathrm{GHz}} / \% P_{1.4\,\mathrm{GHz}}\right)$ and the rotation of the electric vector $\Delta\phi$ ($= \phi_{0.6\,\mathrm{GHz}} - \phi_{1.4\,\mathrm{GHz}}$, measured from the North to the East) were determined.

The r.m.s. noise level was measured from the V-map. Assuming the intrinsic circular polarization to be negligible, the V-map is a measure of the combined effects of receiver noise, part of the instrumental polarization and interference. The $1 - \sigma$ noise level in the appropriate

part (that is where the radio source is) of the *V*-map determines the r.m.s. noise level and has been taken as the uncertainty in the *Q* and *U* maps. But for *Q* and *U* there are additional instrumental terms.

In most cases the effective noise level in the *I*-map is dominated by dynamic range limitations due to differences between the real and predicted synthesized antenna pattern mainly caused by ionospheric and atmospheric disturbances, and incomplete removal of background sources within and outside of the synthesized field, the latter is relatively severe at 0.6 GHz because of the large field of view of the primary beam and the high density of the background sources. In the contour representations of each *I*-map the first contour level was chosen at the lowest reliable intensity in the map. This level was determined taking into account the lowest negative map intensities. To check whether there are systematic effects in the intensity maps (e.g. a negative bowl due to missing short spacings together with an insufficient cleaning), the reduced maps have been compared with older observations described in the literature. Of all radio sources the integrated values of both the total intensity and the polarization have been determined and compared with those interpolated from integrated values measured at other frequencies with various instruments including single dish telescopes. Systematic effects would cause the integrated values to deviate from the interpolated values (in the example above the integrated values would be too small). The integrated values appear to agree well (within the uncertainties) with the interpolated values, which means that no systematic effects are present in the maps. As at long wavelengths the problems of the missing short spacings are much less than those at e.g. 6 cm, this result was expected.

Both the r.m.s. noise and confusion levels in the *I*-map are given in the tables I and III.

The lowest contour levels in the maps of the total intensity and polarization were taken as cut-off levels for the calculation of percentage polarization, spectral index, etc. In general values below these levels were ignored, except to show regions of the source whose polarization was below a specified upper limit.

3. Results.

Figures 1 to 9 show the results.

In each case panel (a) shows a contour plot of the total intensity distribution of the radio source at 0.6 GHz. The dashed contours represent « negative » brightnesses. Superimposed on each map are the position angles of the electric vectors of the lineary polarized intensity with arbitrary lengths. An ellipse represents the half-power intensity of the synthesized beam, and a cross marks the position of the optical galaxy identified with the radio source. Panel (b) shows a contour plot of the linearly polarized intensity distribution at 0.6 GHz superimposed on a two-level gray scale plot of the total intensity distribution. Panel (c) shows a gray scale plot of the distribution of the percentage polarization at 0.6 GHz superimposed on a two-contour plot of the total intensity distribution. Note that for the percentage polarization the first gray values represent upper limits i.e. they indicate regions where the percentage polarization is smaller than the indicated value. Higher levels represent absolute values.

Panels (d), (e) and (f) show the same quantities as (a), (b) and (c) but at 1.4 GHz, that is the distributions of total intensity, the intensity of the linear polarization and the percentage polarization.

Panels (g), (h) and (i) show the distributions of spectral index, depolarization and the rotation of the electric vector superimposed on two-levels plots of the total intensity distribution at 0.6 GHz.

Panel (j) shows the spectral index variation along each radio source. The lower panel shows the integrated (parallel to the minor axis) total intensity along the major axis of the radio source at 0.6 GHz (thick line) and 1.4 GHz (thin line). The two lines have been normalized to the maximum of the 0.6 GHz curve. The upper panel is the spectral index variation. Values with uncertainties larger than 1.0 have been omitted. O Marks the position of the optical galaxy. The points in the curves are not independent as they reflect values with a separation of one grid-point. In general each independent beam comprises 2.8 points in both dimensions.

Table IV lists the integrated values of total intensity, percentage linear polarization and position angle of the electric vector at 0.6 GHz and 1.4 GHz for each source. The integrated values have been determined by summing the pixel intensities in the appropriate part of the maps and then normalizing for the synthesized beam. This was done for the *I*, *Q* and *U*-maps. The values for the integrated percentage polarization and the polarization position angles have been calculated using the integrated *I*, *Q* and *U* values.

The uncertainties in the various quantities have been determined using the R.M.S. noise levels and the confusion levels as given in tables I and III. As mentioned above the integrated percentage polarization can be small although there is locally significant polarization. The uncertainty can therefore be larger than the value itself. In these cases an upper limit is given which is the sum of the value and its uncertainty. The corresponding position angle is then in brackets.

The integrated values derived here at 0.6 GHz and 1.4 GHz agree well with those interpolated from integrated values measured at other frequencies with various instruments including single dish telescopes. This is an indication that the flux density scales are correct and that any departures from zero in the mean level of the cleaned and restored *I*-maps are negligible.

4. Notes on individual sources.

3C33.1

The 5 GHz total intensity map of 3C33.1 by Van Breugel and Jägers (1982) shows two unresolved hot spots in extended emission regions and a narrow elongated bridge located halfway between the core and the southern hot spot. The magnetic field is generally parallel to the jet direction.

The total intensity map at 0.6 GHz shows three peaks at the positions of the two hot spots and the bridge. There is a large difference in spectral index distribution between the northeast and the southwest components. In the southwest component it remains roughly constant to the outer edge. There is also a difference in polarization structure between the northeast and the southwest components of the radio source. Although the integrated polarization intensities of the two components differ by not more than a factor of 2 at 1.4 GHz, at 0.6 GHz it is a factor of ~ 10. The rotation of the polarization position angles is approximately the same in both components. The maxima in the polarization distribution are at the edges of the peaks in the total intensity. Moreover, the fractional polarization increases towards the edge of the radio source. This is a « common » property of radio sources (Van Breugel and Jägers, 1982).

3C35

Van Breugel and Jägers (1982) presented a 5 GHz total intensity map of 3C35 showing two completely resolved lobes. The « hot spot » in the southern lobe appeared to be double. In the northern hot spot the magnetic field is parallel to the northeastern boundary, in the southern it is parallel to the brightest rim of the banana-shaped hot spot (Van Breugel, 1980).

The 0.6 GHz total intensity map shows a symmetrical structure including a central radio component. Except for a few points at the southern edge, the spectral index increases continuously towards the centre, where a dip appears at the central component. The polarization distribution shows small scale structure, at 0.6 GHz there are two separate peaks in the northern component, in the southern one there is a large low intensity region. As in 3C33.1 there is a large difference in the (integrated) depolarization between the two components. The integrated fractional polarization of the northern component at 0.6 GHz is about twice as large as at 1.4 GHz.

The distribution of depolarization and the rotation of the polarization position angles are clumpy. Note that the plotted vectors are independent.

3C111

Högbom (1979) showed that the radio source 3C111 has a triple structure at 5 GHz with an unresolved central radio component. The projected magnetic field in the northeast lobe, in contrast to that in the associated tail of emission, is directed nearly at right angles to the main axis of the source. The field in the southwest lobe appears to follow the western edge of the low level extension towards the north.

At 0.6 GHz there is a central radio component visible at the position of the galaxy and a large region of low brightness emission to the northwest. The course of the spectral index is different from that in 3C33.1 and 3C35. In the West the spectral index increases towards the outer edge. To the East it first increases and then decreases again. The central component is distinguished by a relatively small spectral index.

The polarization structure has two peaks just at the edges of the outer peaks in the total intensity. The low brightness region appears to be not significantly polarized. The (integrated) fractional polarization of the eastern hot spot at 0.6 GHz is about 4 times that at 1.4 GHz, while that of the western hot spot remains about constant. The distribution in the rotation of the polarization angle can be divided into two regions with more or less uniform rotation angles.

B0844+316

Radio maps at 5 GHz of B0844+316 by Van Breugel and Miley (1977) show that a jet is visible in the northern lobe going from the unresolved core to the hot spot. No jet is visible in the southern part of the radio source. It has been suggested that the magnetic field directions are roughly circumferential in both the northern and southern lobes.

The 0.6 GHz and 1.4 GHz radio maps show a double source with low intensity regions along its eastern side. In both components the spectral index seems to increase towards the north. At the position of the known flat-spectrum nucleus again a small dip appears.

The polarization is very asymmetric, in structure as well as in integrated fractional polarization. The difference in the latter is more than a factor of 30. The depolarization distribution in the southern lobe is remarkable : there are two regions with $DP > 1$, separated by a region with $DP < 1$.

3C223

Högbom (1979) showed that at 5 GHz a triple structure exists in 3C223, containing a central unresolved radio component. There is evidence that the magnetic field is aligned with the boundaries of the lobes.

At 0.6 GHz the radio structure is very regular and symmetric. The central radio component is not visible in the radio maps but the spectral index shows a dip at that position. Again the spectral index increases towards the centre in both components.

3C223 is extremely highly polarized at 0.6 GHz compared with the other sources. The three polarization peaks at 1.4 GHz are less visible at 0.6 GHz. The two strongest peaks remain at the edges of the hot spots. The fractional polarization is about the same in both hot spots. At 0.6 GHz the fractional polarization is higher than at 1.4 GHz in the northern component. The rotation of the polarization position angle is about constant over the source except for a small region South of the North hot spot. This region coincides with the third (weaker) peak at 1.4 GHz.

4C26.35A

Previous published maps of 4C26.35A at 1.4 GHz (Riley, 1975) and at 2.7 GHz (Owen *et al.*, 1977) show a quadrupole structure as in 3C452.

The radio maps at 0.6 GHz show a « simple » double structure. There appears to be an appreciable amount of polarization at 0.6 GHz, especially in the northwestern half of the source, where the fractional polarization increases towards the outer edges. The difference in integrated polarization between either side of the nucleus is only about 2 which is much less than in the other

sources. The polarization position angles suggest that in the northwestern component there is a circumferential magnetic field. In the southeastern component there are two regions with different angles. 4C26.35A has a close companion 4C26.35B (Riley, 1975) to the northeast. Both sources are shown in the figures.

4C74.17.1

Van Breugel and Willis (1981) showed that at 5 GHz a jet is visible in the northern bridge emanating from the unresolved nuclear radio component of the source. In the south only an extended region is visible, but there is no counterjet. They found that the magnetic field is directed along the jet over its entire length. At 0.6 GHz we see a triple radio source, the middle component of which coincides with the jet. The spectral index increases continuously towards the north in contrast with the high resolution spectral index of the jet between 1.4 GHz and 5.0 GHz. In the two outer lobes the spectral index increases towards the middle component.

Only at the edges of the components is there some significant polarization at 0.6 GHz. In all three components there is appreciable depolarization. The (integrated) depolarization is about the same in the outer lobes.

3C390.3

Hargrave and Mc Ellin (1975) showed that at 5 GHz the northern component of the triple radio source 3C390.3 has a plateau of emission of low surface brightness surmounted by two principal features. The southern component has a partially resolved head and tail. The central component is unresolved. Harris (1971) showed that the dominant part of the magnetic field is ordered in a direction parallel to the axis of the respective components of the source. The distribution of the spectral index is different from that in the other sources. In the northern lobe it is roughly straight, with perhaps a small increase towards the outer edge. In the southern lobe it increases towards the centre of the lobe from both sides.

The polarization structure reveals five features (see also Jägers and Ma, 1983). At 1.4 GHz the integrated fractional polarization is equal, within a factor of 2, in the southern and northern components. However, at 0.6 GHz the difference is enormous. The depolarization in the southern component is smaller than 0.1. The rotation of the polarization position angle differs between the various components.

3C452

The structure of 3C452 at 5 GHz resembles that of 3C223 (Högbom, 1979), it being a triple radio source with an unresolved central component coincident with the parent galaxy. The magnetic field direction is clearly related to edges and elongated features in the radio maps. The slight tendency to distortion with rotational symmetry in the extended emission region of this source is also seen in the projected magnetic field configuration.

At 0.6 GHz a quadrupole structure is visible. The distribution of the spectral index along the radio source is roughly similar to that in 3C223.

The polarization structure in the eastern and western parts of the source is about the same, just as the (integrated) fractional polarization. At 1.4 GHz the differences are large. Therefore, the depolarization distribution is also asymmetric. The rotation of the polarization position angle is clumpy.

Acknowledgements.

I thank the staff of the Westerbork Synthesis Radio Telescope and the Reduction Group for their work on these observations. The Westerbork Radio Observatory is operated by the Netherlands Foundation for Radio Astronomy with the financial support of the Netherlands Organization for the Advancement of pure Research (ZWO). I acknowledge useful discussions with H. van der Laan, G. K. Miley and R. G. Strom. I also thank W. Brokaar and J. Ober for preparation of the figures.

References

BAARS, J. W. M., HOOGHOUDT, B. G. : 1974, *Astron. Astrophys.* **31,** 323.
ELSMORE, B., RYLE, M. : 1976, *Mon. Not. R. Astron. Soc.* **174,** 411.
HARGRAVE, P. J., MC ELLIN, M. : 1975, *Mon. Not. R. Astron. Soc.* **173,** 37.
HARRIS, A. : 1971, *Mon. Not. R. Astron. Soc.* **158,** 1.
HÖGBOM, J. A. : 1974, *Astron. Astrophys. Suppl. Ser.* **15,** 147.
HÖGBOM, J. A., BROUW, W. N. : 1974, *Astron. Astrophys.* **33,** 289.
HÖGBOM, J. A., CARLSSON, I. : 1974, *Astron. Astrophys.* **34,** 341.
HÖGBOM, J. A. : 1979, *Astron. Astrophys. Suppl. Ser.* **36,** 173.
JÄGERS, W. J., MA, E. : 1983, *Acta Astron. Sinica* **29,** 360.
MILEY, G. K. : 1980, *Ann. Rev. Astron. Astrophys.* **18,** 165.
OWEN, F. N., RUDNICK, L., PETERSON, B. M. : 1977, *Astron. J.* **82,** 677.
RILEY, J. M. : 1975, *Mon. Not. R. Astron. Soc.* **170,** 53.
SPOELSTRA, T. A. T. : 1983, *Astron. Astrophys.* **120,** 313.
VAN BREUGEL, W. J. M., MILEY, G. K. : 1977, *Nature* **265,** 315.
VAN BREUGEL, W. J. M. : 1980, *Astron. Astrophys.* **81,** 275.
VAN BREUGEL, W. J. M., WILLIS, A. G. : 1981, *Astron. Astrophys.* **96,** 332.
VAN BREUGEL, W., JÄGERS, W. : 1982, *Astron. Astrophys. Suppl. Ser.* **49,** 529.
VAN SOMEREN-GRÈVE, H. W. : 1974, *Astron. Astrophys. Suppl. Ser.* **15,** 343.
WILLIS, A. G., STROM, R. G., BRIDLE, A. H., FAMALONT, E. B. : 1981, *Astron. Astrophys.* **95,** 250.

TABLE I. — *Observational parameters.*

Source	Alternative Name	Field Centre RA(1950) H M S	Field Centre DEC(1950) D M S	Field Centre l D	Field Centre b D	Observing Date YR Day	Receiver	Halfpower Beam(arcs) RA x DEC	RMS Noise mJy/bm	Confusion Level I-map mJy/bm
(1)	(2)	(3)	(4)	(5)	(6)	(7)	(8)	(9)	(10)	(11)
0106+729	3C33.1	01 06 00	72 55 30	124.3	10.4	82 029	new	29 x 30	0.7	10.0
0109+429	3C35	01 10 00	49 10 00	126.5	-13.3	80 333	old	29 x 38	1.0	2.5
0415+379	3C111	04 15 00	37 54 00	161.7	-8.8	82 023	new	29 x 47	0.4	50.0
0844+316	B2	08 44 51	31 58 45	192.2	37.5	82 082	new	29 x 55	0.4	5.0
0936+361	3C223	09 36 51	36 07 35	188.4	48.7	82 080	new	29 x 49	0.4	2.0
1155+266	4C26.35A	11 55 45	26 38 00	231.6	78.1	82 017	new	29 x 65	0.4	4.0
1209+745	4C74.17.1	12 09 30	74 36 20	126.5	42.5	82 040	new	29 x 30	0.4	2.5
1845+797	3C390.3	18 45 30	79 43 00	111.4	27.1	81 172	old	29 x 29	1.3	20.0
2243+394	3C452	22 43 30	39 26 00	98.1	-17.1	82 026/040	new	29 x 46	0.7	25.0

TABLE II. — *Calibration sources (Elsmore and Ryle, 1976).*

Source	Assumed Position (1950.0) RA H M S	DEC H M S	Assumed Flux Densities I Jy	Q Jy	U Jy
(1)	(2)	(3)	(4)	(5)	(6)
3C48	01 34 49.826	32 54 20.52	28.07	0.00	0.01
3C147	05 38 43.506	49 49 42.83	37.78	0.00	0.00
3C286	13 28 49.654	30 45 58.70	20.52	-0.41	-0.29
3C309.1	14 58 56.644	71 52 11.15	13.02	0.03	0.03
3C380	18 28 13.516	48 42 40.87	26.26	-0.36	0.02

TABLE III. — *Relevant parameters of the additional 1.4 GHz observations.*

Source	Alternative Name	Frequency and Bandwidth MHz	MHz	Observing Date YR Day	RMS Noise mJy/bm	Confusion Level I-map mJy/bm	Notes
(1)	(2)	(3)	(4)	(5)	(6)	(7)	(8)
0106+729	3C33.1	1412.625	10	77 294/360	0.2	5.0	a
0109+492	3C35	1412	10	78 008	0.2	1.0	a
0415+379	3C111	1415	4	77 175	0.4	10.0	b
0849+316	B2	1415	4	74 182	0.5	2.5	c
0936+361	3C223	1415	4	77 175/184	0.4	10.0	a
1155+266	4C26.35A						d
1209+745	4C74.17.1	1415	4	77 190	0.3	0.5	e
1845+797	3C390.3	1415	4	71 265	1.1	15.0	f
2243+394	3C456	1415	4	71 109	1.0	20.0	b

Notes to table III :

([a]) VAN BREUGEL, W., JÄGERS, W. : 1982, *Astron. Astrophys. Suppl. Ser.* **49,** 529.

([b]) HÖGBOM, J. A., CARLSSON, I. : 1974, *Astron. Astrophys.* **34,** 341.

([c]) VAN BREUGEL, W. J. M., MILEY, G. K. : 1977, *Nature* **265,** 315.

([d]) no observations at 1.4 GHz.

([e]) VAN BREUGEL, W. J. M., WILLIS, A. G. : 1981, *Astron. Astrophys.* **96,** 332.

([f]) MILEY, G. K., VAN DER LAAN, H. : 1973, *Astron. Astrophys.* **28,** 359.

TABLE IV. — *Integrated parameters.*

Source	Alternative Name	0.6 GHz Total Flux Density Jy	0.6 GHz Percentage Polarization %	0.6 GHz Polarization Position Angle Degrees	1.4 GHz Total Flux Density Jy	1.4 GHz Percentage Polarization %	1.4 GHz Polarization Position Angle Degrees
(1)	(2)	(3)	(4)	(5)	(6)	(7)	(8)
0106+729	3C33.1	6.47 ± 0.18	1.4 ± 0.2	144 ± 4	3.29 ± 0.09	3.4 ± 0.1	95 ± 1
0109+492	3C35	4.58 ± 0.13	2.9 ± 1.1	163 ±11	2.34 ± 0.05	3.5 ± 0.4	77 ± 4
0415+379	3C111	27.75 ± 0.99	1.2 ± 0.1	76 ± 1	15.37 ± 0.20	1.7 ± 0.1	88 ± 1
0844+516	B2	2.77 ± 0.09	0.3 ± 0.2	155 ±21	1.43 ± 0.05	1.3 ± 0.6	19 ±13
0936+361	3C223	6.91 ± 0.16	7.7 ± 0.6	121 ± 2	3.57 ± 0.16	7.7 ± 0.4	120 ± 1
1155+266	4C26.35A	2.17 ± 0.08	0.8 ± 0.3	91 ±10			
1209+745	4C74.17.1	1.21 ± 0.07	< 3.6	(33 ±1)	0.59 ± 0.01	1.8 ± 1.3	94 ± 1
1845+797	3C390.3	20.24 ± 0.38	2.1 ± 0.1	58 ± 2	10.53 ± 0.29	6.3 ± 0.3	4 ± 1
2243+394	3C452	22.57 ± 0.49	0.2 ± 0.1	1 ± 9	11.06 ± 0.39	5.5 ± 0.3	26 ± 1

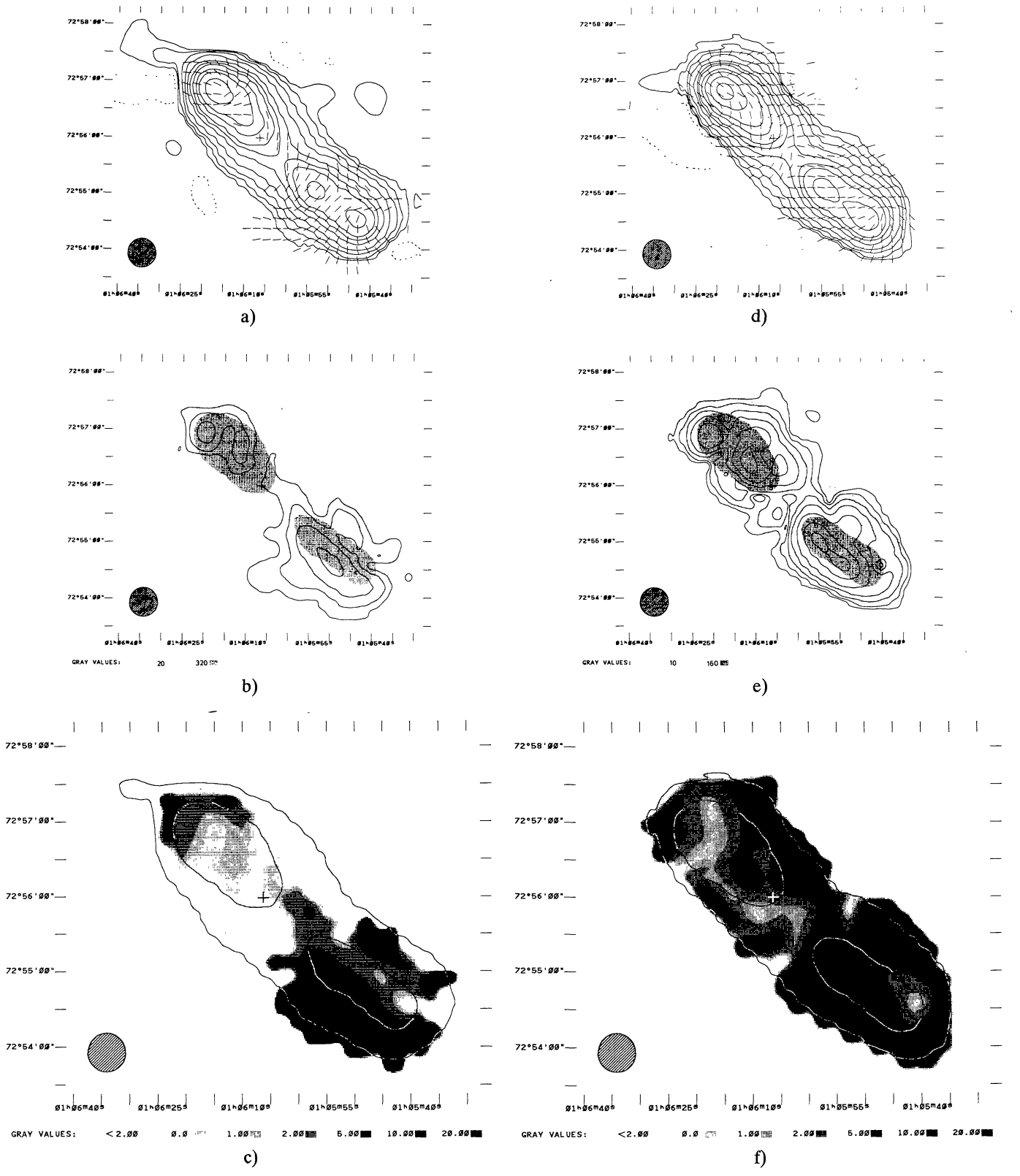

FIGURE 1. — (a) The total intensity distribution of 3C33.1 at 0.6 GHz. The contour levels are – 10, 10, 20, 40, 80, 160, 240, 320, 480, 640 and 960 mJy/beam. (b) The linearly polarized intensity distribution of 3C33.1 at 0.6 GHz. The contour levels are 5, 10, 20 and 40 mJy/beam. (c) The distribution of the percentage polarization of 3C33.1 at 0.6 GHz. The two levels in the total intensity contour map are 20 and 320 mJy/beam. (d) The total intensity distribution of 3C33.1 at 1.4 GHz. The contour levels are – 5, 5, 10, 20, 40, 80, 120, 160, 240, 320, 480 and 640 mJy/beam. (e) The linearly polarized intensity distribution of 3C33.1 at 1.4 GHz. The contour levels are 0.75, 1.5, 3, 6, 12, 24 and 36 mJy/beam. (f) The distribution of percentage polarization of 3C33.1 at 1.4 GHz. The two levels in the total intensity contour map are 10 and 160 mJy/beam.

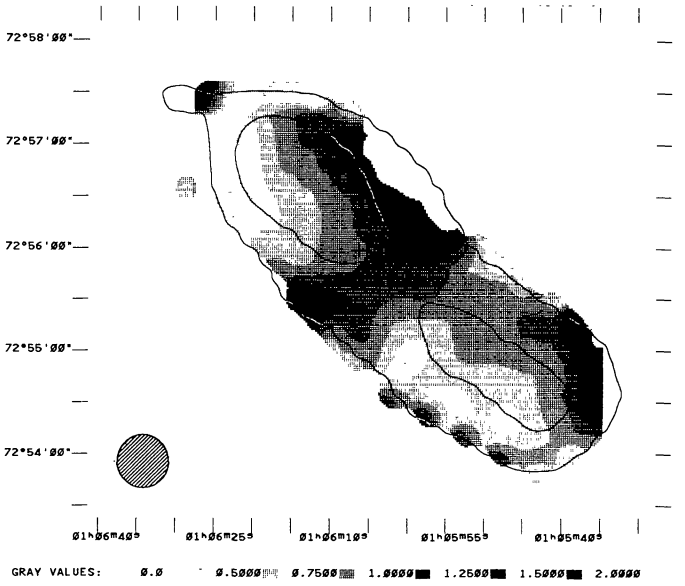

g)

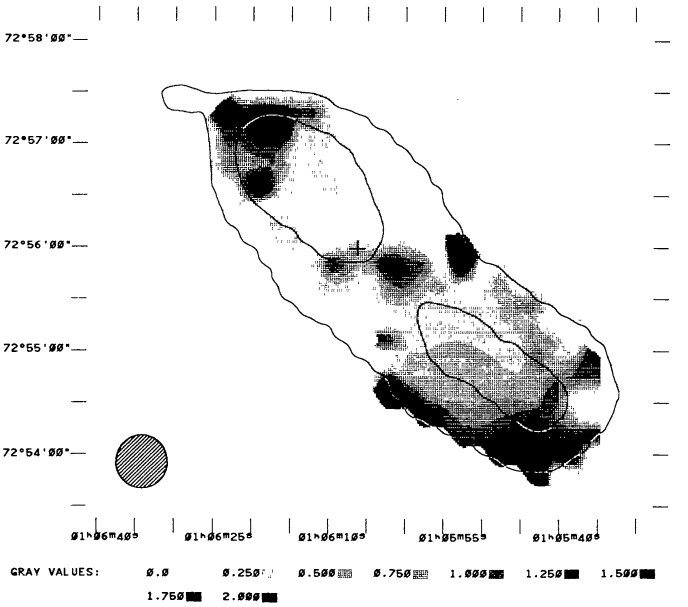

h)

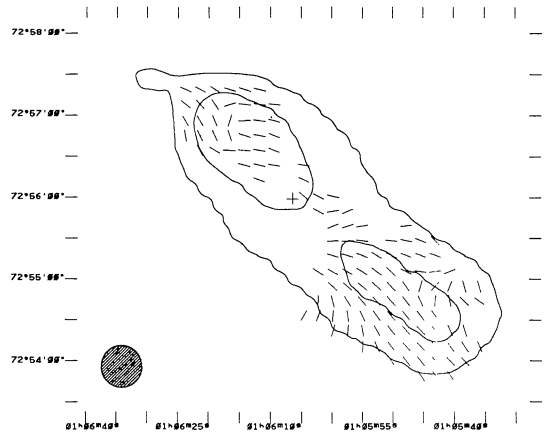

i)

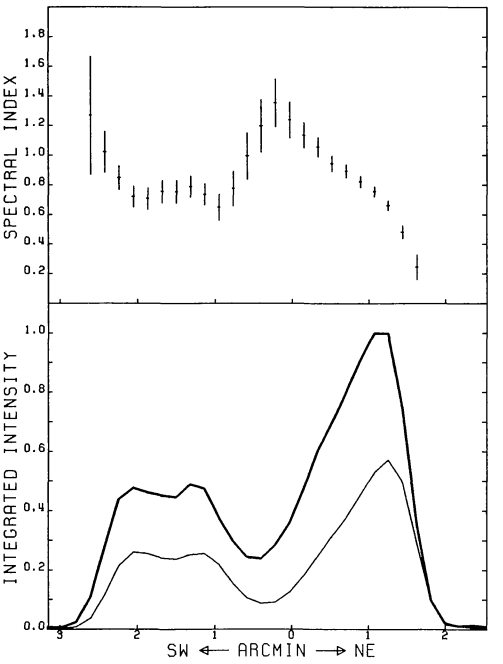

j)

FIGURE 1. — (g) The distribution of the spectral index of 3C33.1 between 0.6 GHz and 1.4 GHz. The two levels in the total intensity contour map at 0.6 GHz are 20 and 320 mJy/beam. (h) The distribution of the depolarization of 3C33.1 between 0.6 GHz and 1.4 GHz. The two levels in the total intensity contour map at 0.6 GHz are 20 and 320 mJy/beam. (i) The distribution of the rotation of the polarization position angle of 3CC33.1 between 0.6 GHz and 1.4 GHz measured from the North towards the East. The two levels in the total intensity contour map at 0.6 GHz are 20 and 320 mJy/beam. (j) The spectral index variations along the major axis of 3C33.1 between 0.6 GHz and 1.4 GHz. The lower panel shows the integrated total intensity along the radio source at 0.6 GHz (thick line) and 1.4 GHz (thin line). The upper panel shows the variations of the spectral index along the radio source.

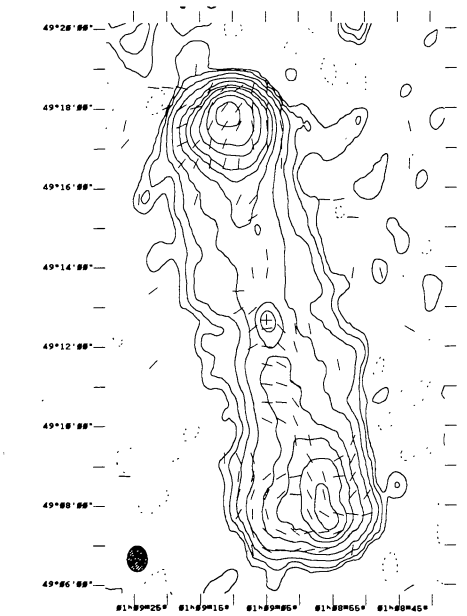

a)

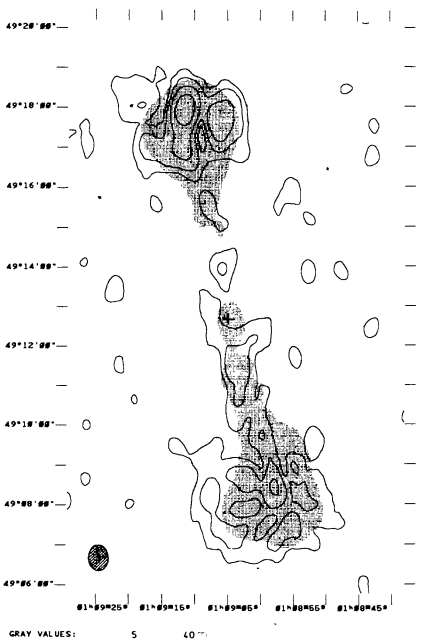

b)

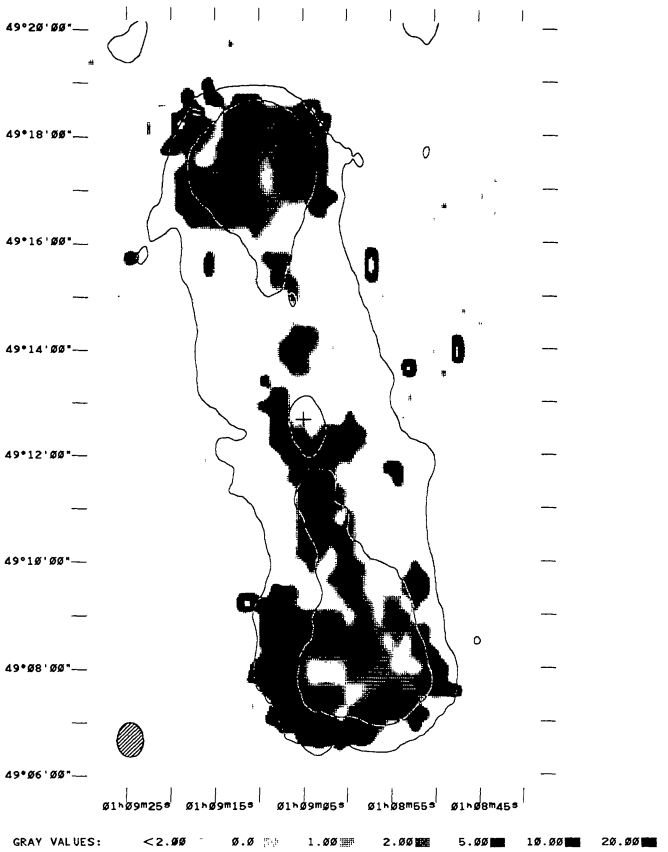

c)

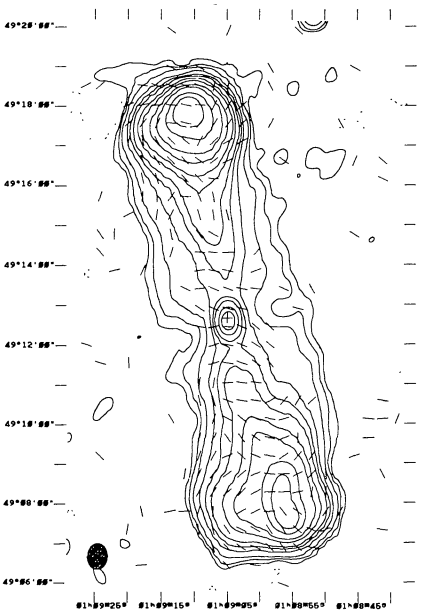

d)

FIGURE 2. — (a) The total intensity distribution of 3C35 at 0.6 GHz. The contour levels are – 2.5, 2.5, 5, 10, 20, 40, 60, 80, 120, 160 and 240 mJy/beam. (b) The linearly polarized intensity distribution of 3C35 at 0.6 GHz. The contour levels are 3, 6, 12 and 24 mJy/beam. (c) The distribution of the percentage polarization of 3C35 at 0.6 GHz. The two levels in the total intensity contour map are 5 and 40 mJy/beam. (d) The total intensity distribution of 3C35 at 1.4 GHz. The contour levels are – 1, 1, 2, 4, 8, 12, 16, 24, 32, 48, 64, 96 and 128 mJy/beam.

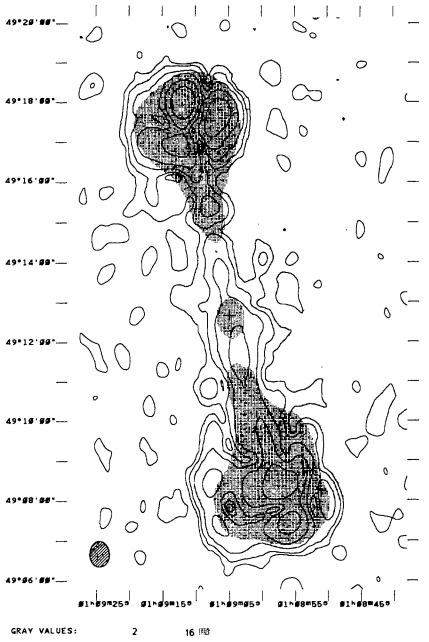

e)

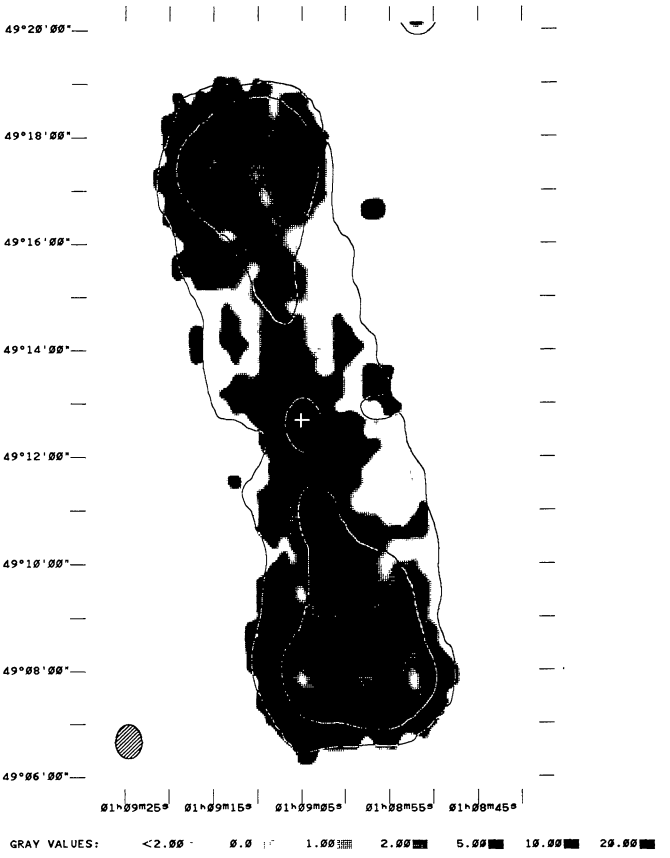

f)

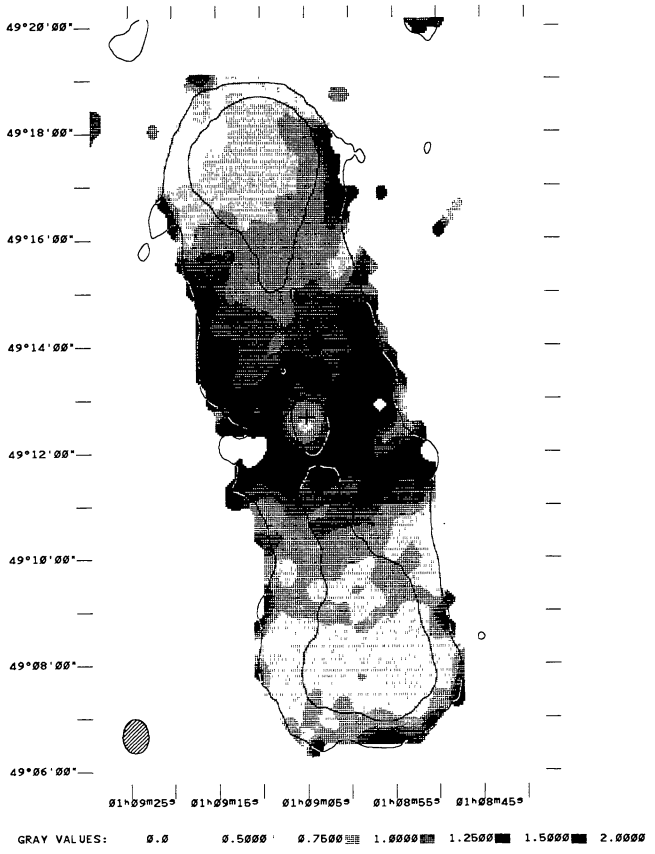

g)

FIGURE 2. — (e) The linearly polarized intensity distribution of 3C35 at 1.4 GHz. The contour levels are 0.5, 1, 2, 4, 8 and 16 mJy/beam. (f) The distribution of the percentage polarization of 3C35 at 1.4 GHz. The two levels in the total intensity contour map are 2 and 16 mJy/beam. (g) The distribution of the spectral index of 3C35 between 0.6 GHz and 1.4 GHz. The two levels in the total intensity contour map at 0.6 GHz are 5 and 40 mJy/beam.

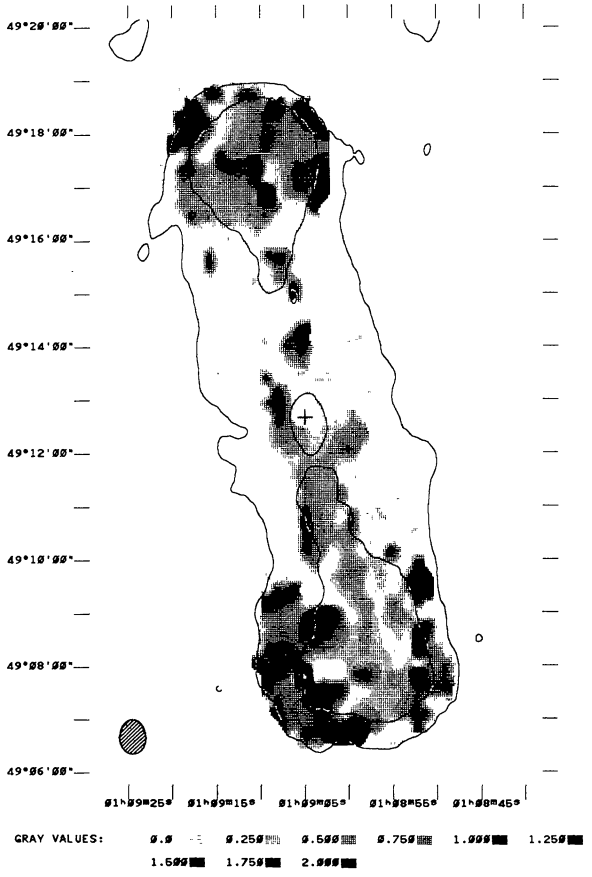

h)

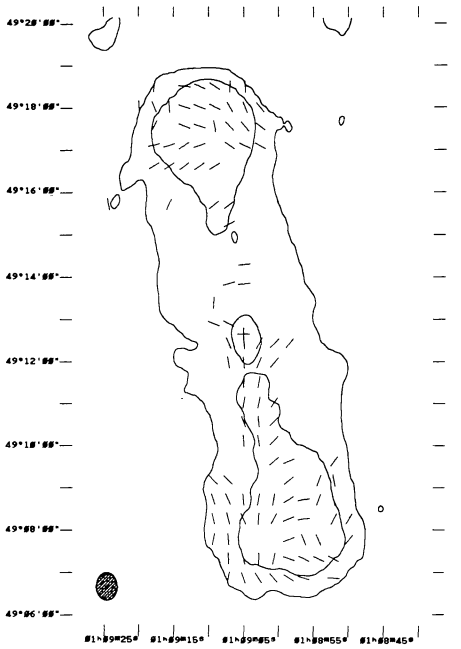

i)

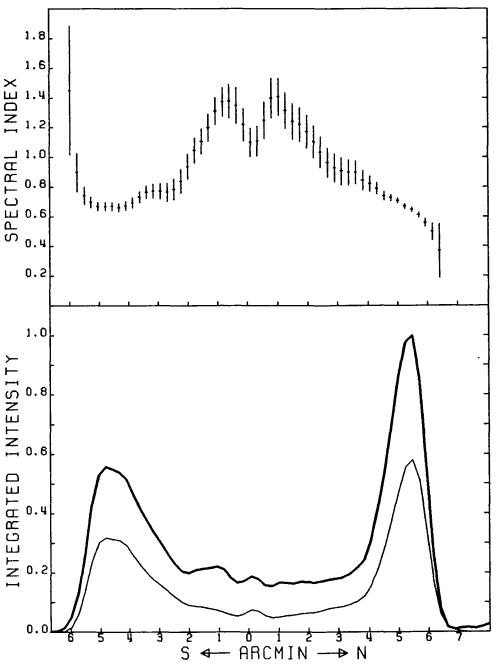

j)

FIGURE 2. — (h) The distribution of the depolarization of 3C35 between 0.6 GHz and 1.4 GHz. The two levels in the total intensity contour map at 0.6 GHz are 5 and 40 MJy/beam. (i) The distribution of the rotation of the polarization position angle of 3C35 between 0.6 GHz and 1.4 GHz measured from the North towards the East. The two levels in the total intensity contour map at 0.6 GHz are 5 and 40 mJy/beam. (j) The spectral index variations along the major axis of 3C35 between 0.6 GHz and 1.4 GHz. The lower panel shows the (integrated) total intensity along the radio source at 0.6 GHz (thick line) and at 1.4 GHz (thin line). The upper panel shows the variations of the spectral index along the radio source.

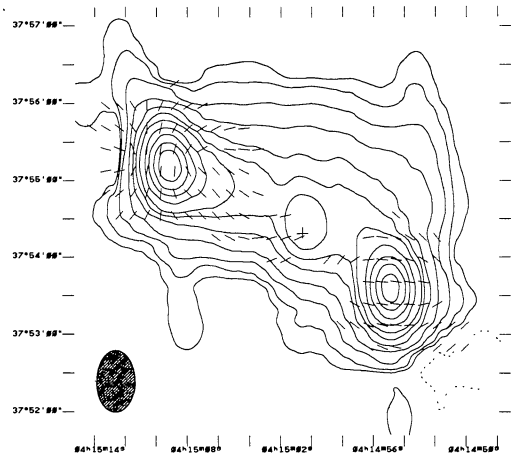

a)

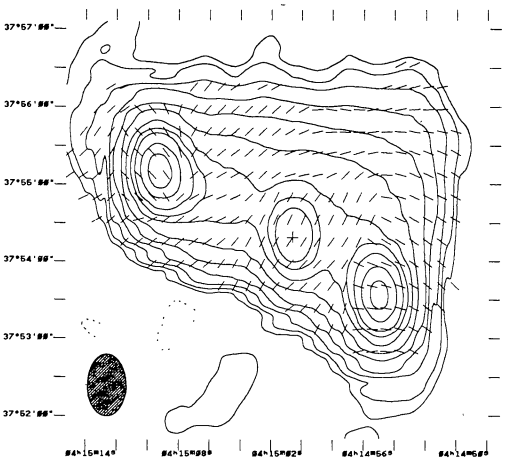

d)

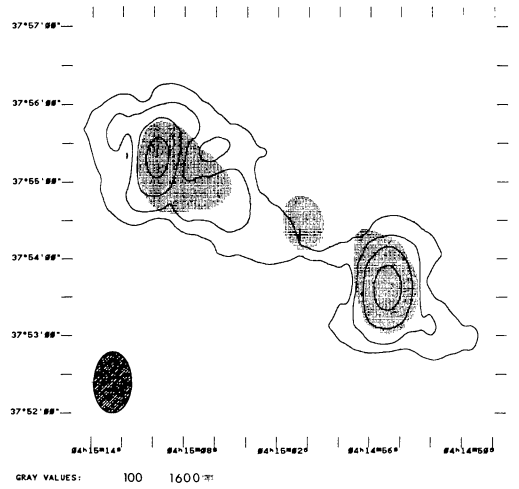

b)

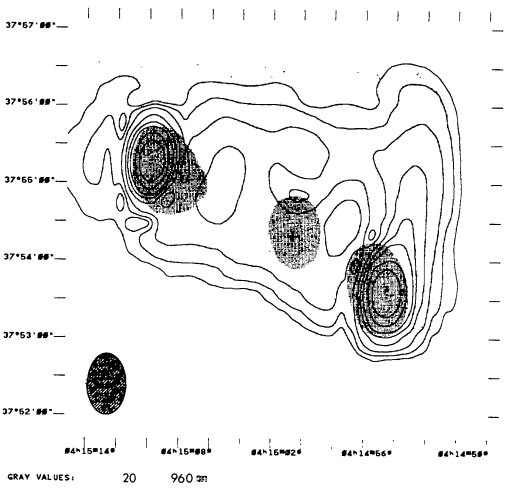

e)

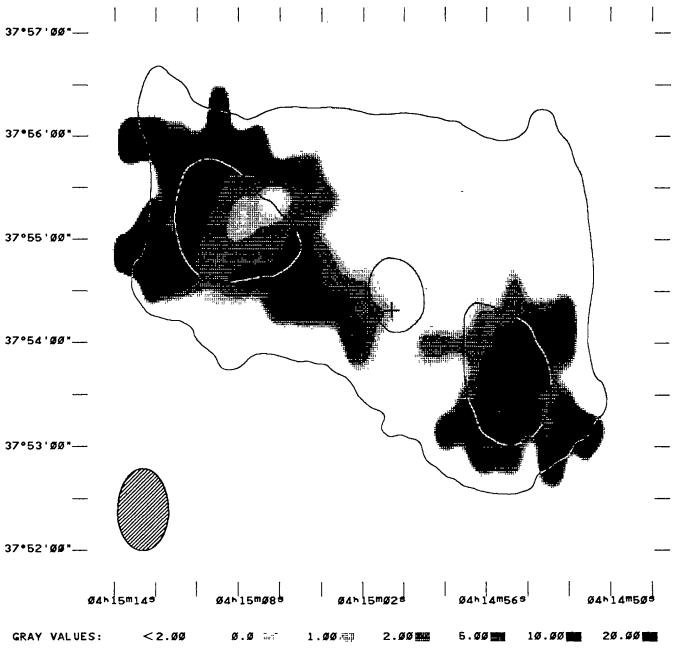

c)

FIGURE 3. — (a) The total intensity distribution of 3C111 at 0.6 GHz. The contour levels are – 50, 50, 100, 200, 400, 800, 1200, 1600, 2400, 3200, 4000 and 4800 mJy/beam. (b) The linearly polarized intensity distribution of 3C111 at 0.6 GHz. The contour levels are 30, 60, 120 and 240 mJy/beam. (c) The distribution of 3C111 at 0.6 GHz. The two levels in the total intensity contour map are 100 and 1600 mJy/beam. (d) The total intensity distribution of 3C111 at 1.4 GHz. The contour levels are – 10, 10, 20, 40, 80, 160, 320, 640, 960, 1280, 1920 and 2560 mJy/beam. (e) The linearity polarized intensity distribution of 3C111 at 1.4 GHz. The contour levels are 5, 10, 20, 40, 60, 80, 120 and 160 mJy/beam.

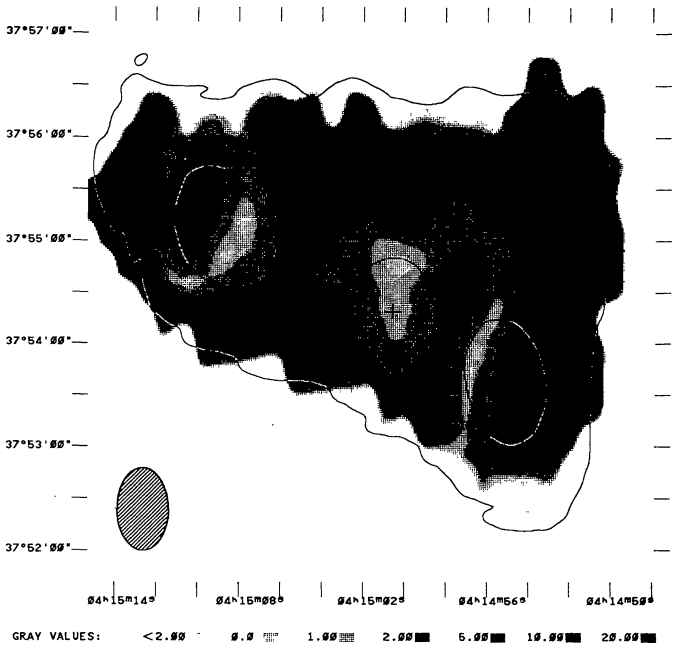

f)

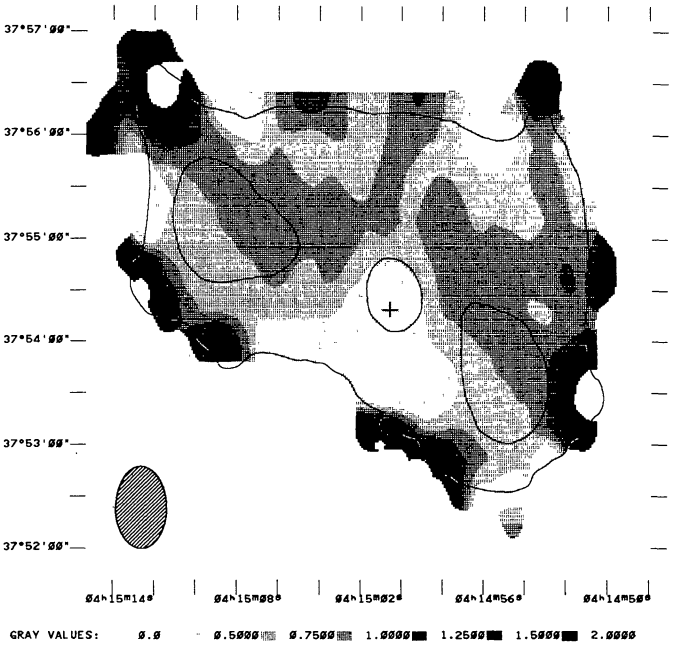

g)

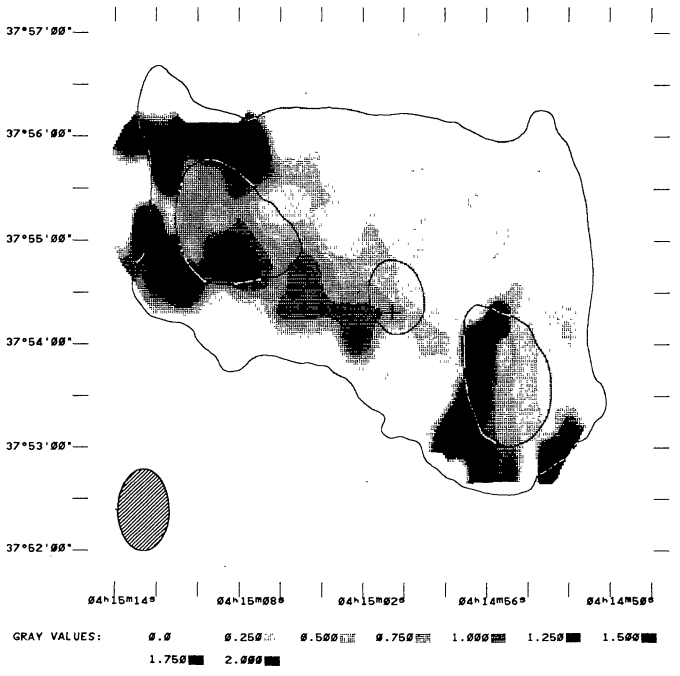

h)

FIGURE 3. — (f) The distribution of the percentage polarization of 3C111 at 1.4 GHz. The two levels in the total intensity contour map are 20 and 960 mJy/beam. (g) The distribution of the spectral index of 3C111 between 0.6 GHz and 1.4 GHz. The two levels in the total intensity contour map at 0.6 GHz are 100 and 1600 mJy/beam. (h) The distribution of the depolarization of 3C111 between 0.6 GHz and 1.4 GHz. The two levels in the total intensity contour map at 0.6 GHz are 100 and 1600 mJy/beam.

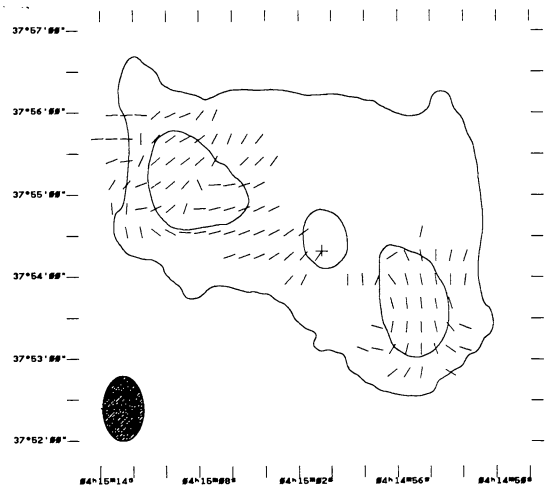

i)

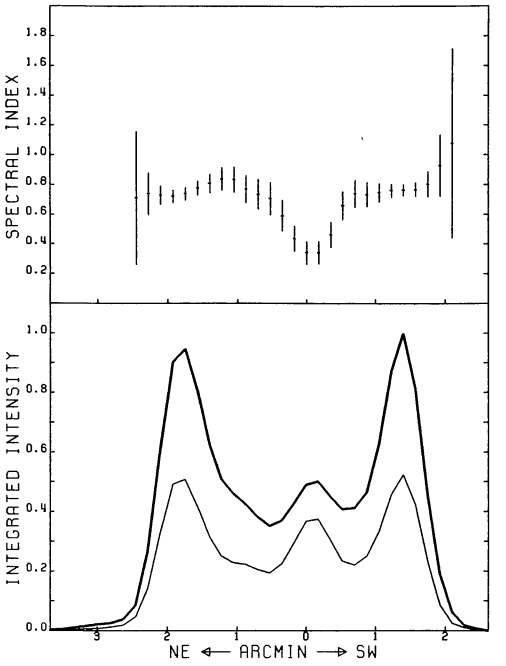

j)

FIGURE 3. — (i) The distribution of the rotation of the polarization position angle of 3C111 between 0.6 GHz and 1.4 GHz measured from the North towards the East. The two levels in the total intensity contour map at 0.6 GHz are 100 and 1600 mJy/beam. (j) The spectral index variations along the major axis of 3C111 between 0.6 GHz and 1.4 GHz. The lower panel shows the (integrated) total intensity along the radio source at 0.6 GHz (thick line) and at 1.4 GHz (thin line). The upper panel shows the variations of the spectral index along the radio source.

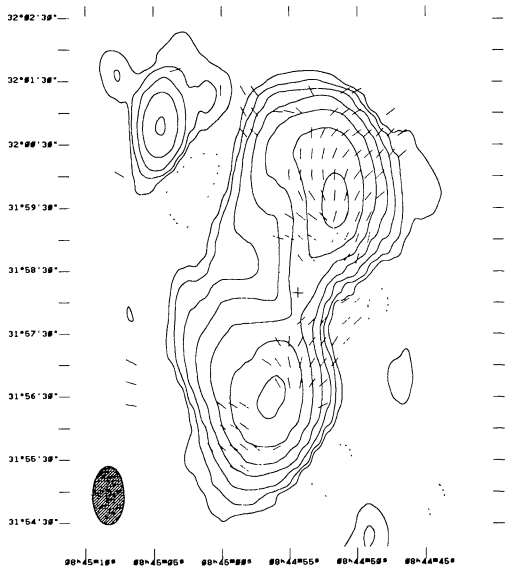

a)

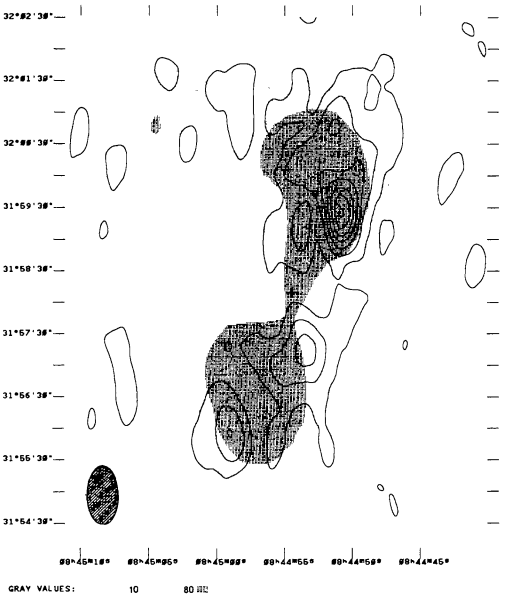

b)

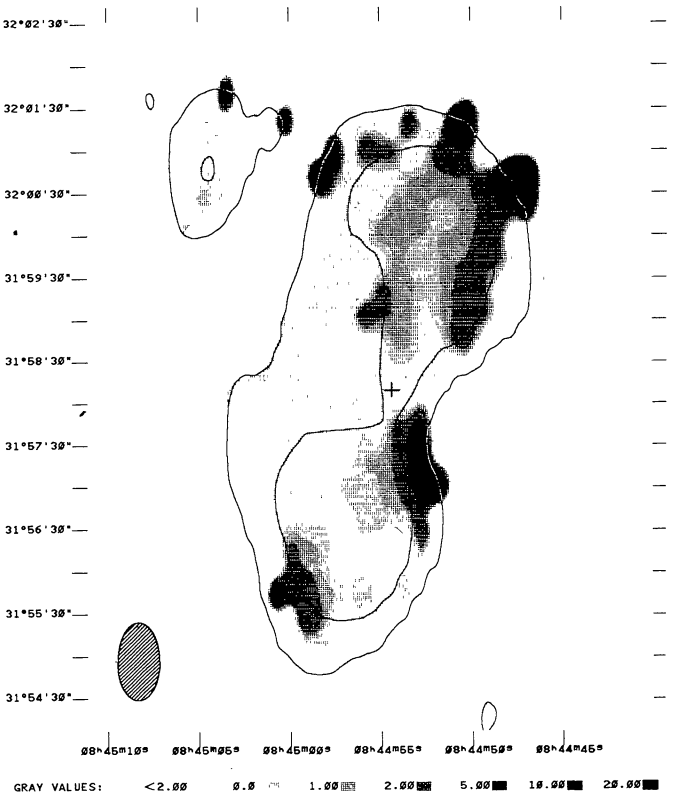

c)

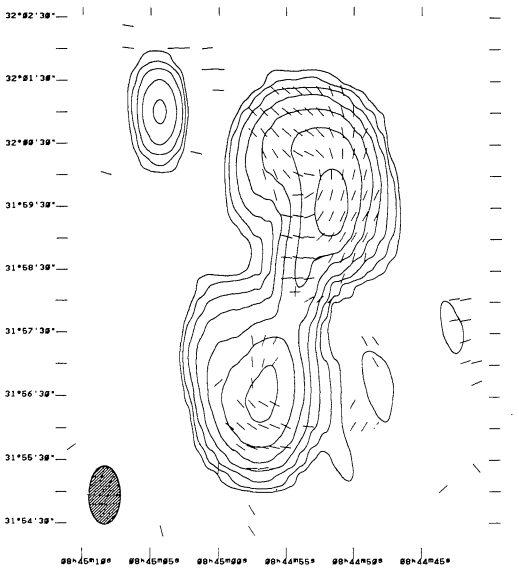

d)

FIGURE 4. — (a) The total intensity distribution of B0844+316 at 0.6 GHz. The contour levels are – 5, 5, 10, 20, 40, 80, 160 and 320 mJy/beam. (b) The linearly polarized intensity distribution of B0844+316 at 0.6 GHz. The contour levels are 1, 2, 3, 4, 5, 6 and 7 mJy/beam. (c) The distribution of the percentage polarization of B0844+316 at 0.6 GHz. The two levels in the total intensity contour map are 10 and 80 mJy/beam. (d) The total intensity distribution of B0844+316 at 1.4 GHz. The contour levels are 1.25, 2.5, 5, 10, 20, 30, 80 and 160 mJy/beam.

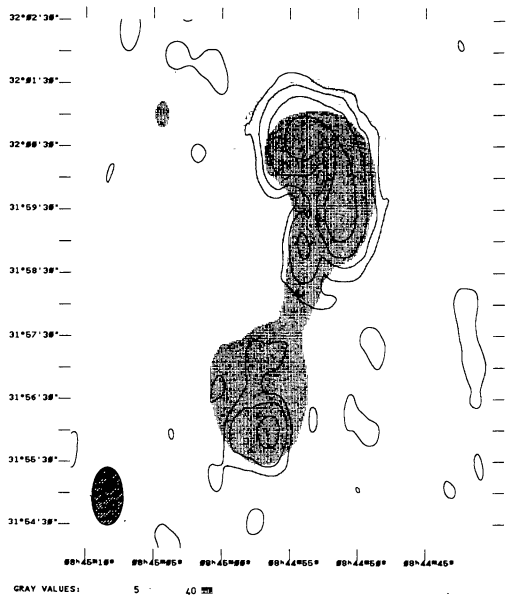

e)

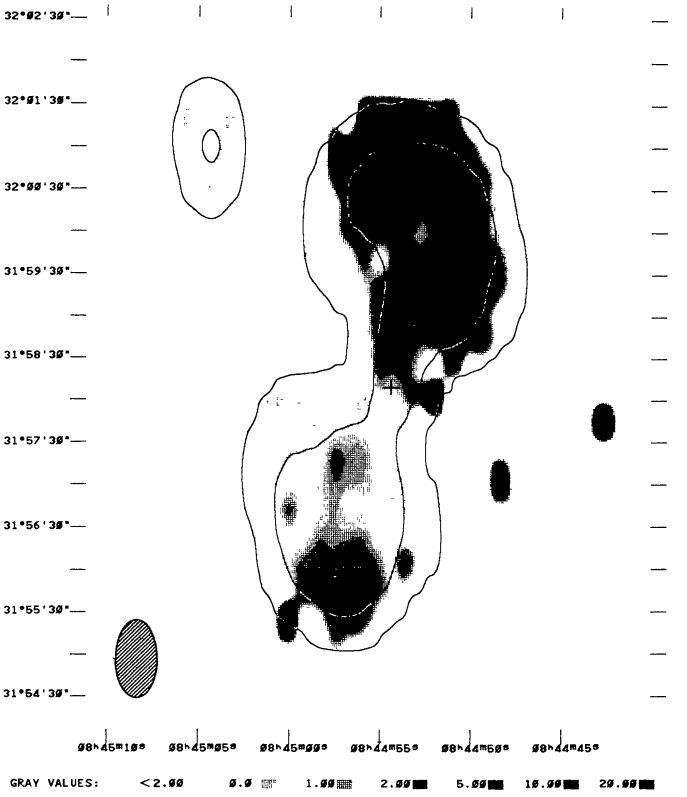

f)

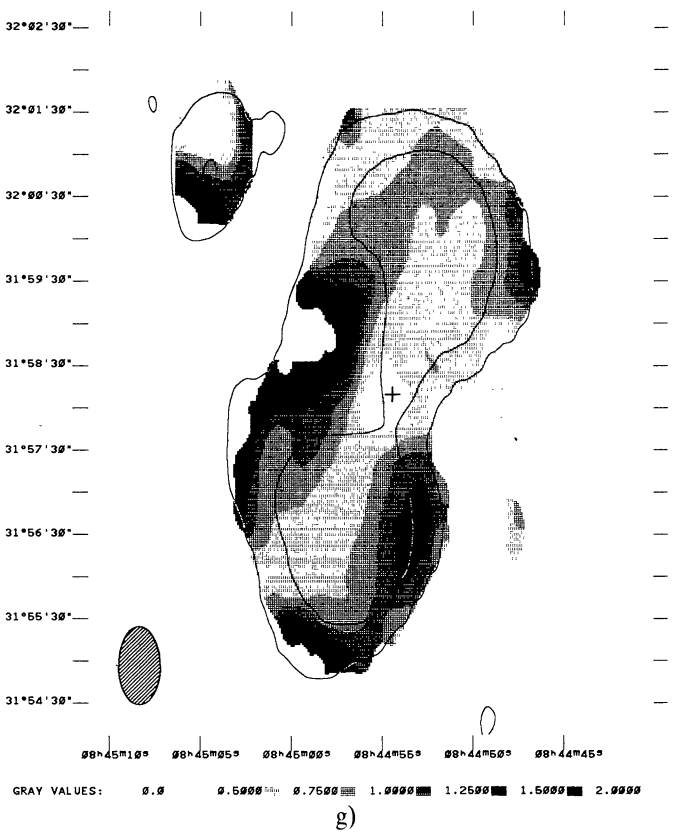

g)

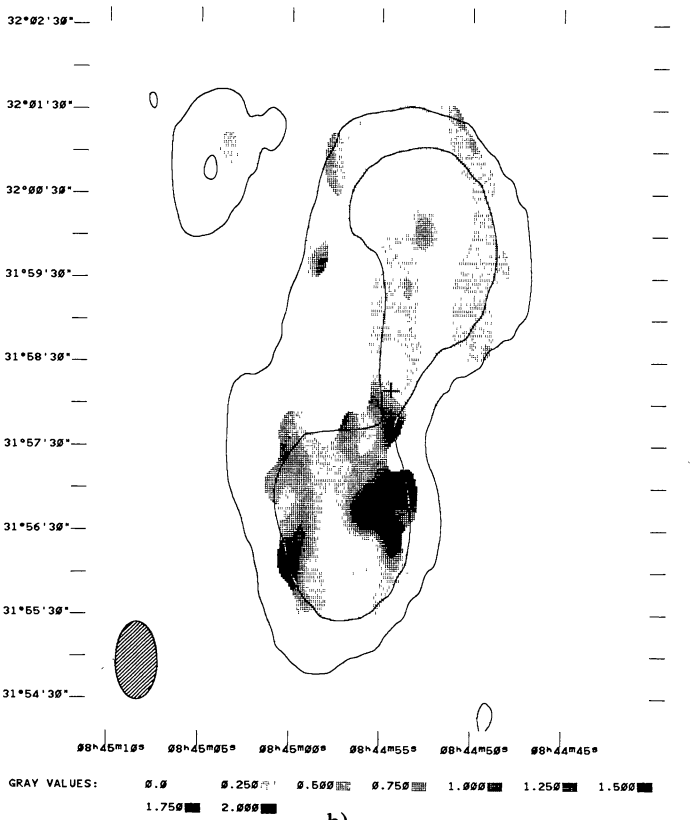

h)

FIGURE 4. — (e) The linearly polarized intensity distribution of B0844+316 at 1.4 GHz. The contour levels are 1.25, 2.5, 5 and 10 mJy/beam. (f) The distribution of the percentage polarization of B0844+316 at 1.4 GHz. The two levels in the total intensity contour map are 5 and 40 mJy/beam. (g) The distribution of the spectral index of B0844+316 between 0.6 GHz and 1.4 GHz. The two levels in the total intensity contour map at 0.6 GHz are 10 and 80 mJy/beam. (h) The distribution of the depolarization of B0844+316 between 0.6 GHz and 1.4 GHz. The two levels in the total intensity contour map are 10 and 80 mJy/beam.

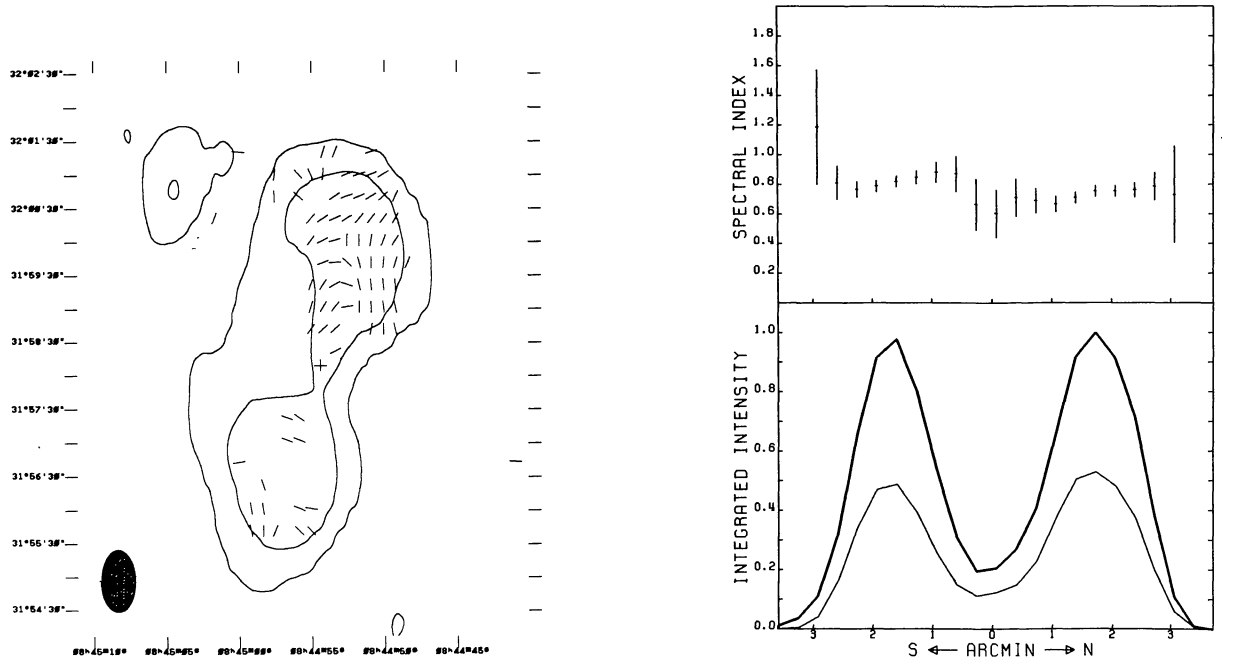

FIGURE 4. — (i) The distribution of the rotation of the polarization position angle of B0844+316 between 0.6 GHz and 1.4 GHz measured from the North towards the East. The two levels in the total intensity contour map at 0.6 GHz are 10 and 80 mJy/beam. (j) The spectral index variations along the major axis of B0844+316 between 0.6 GHz and 1.4 GHz. The lower panel shows the (integrated) total intensity along the radio source at 0.6 GHz (thick line) and at 1.4 GHz (thin line). The upper panel shows the variations of the spectral index along the radio source.

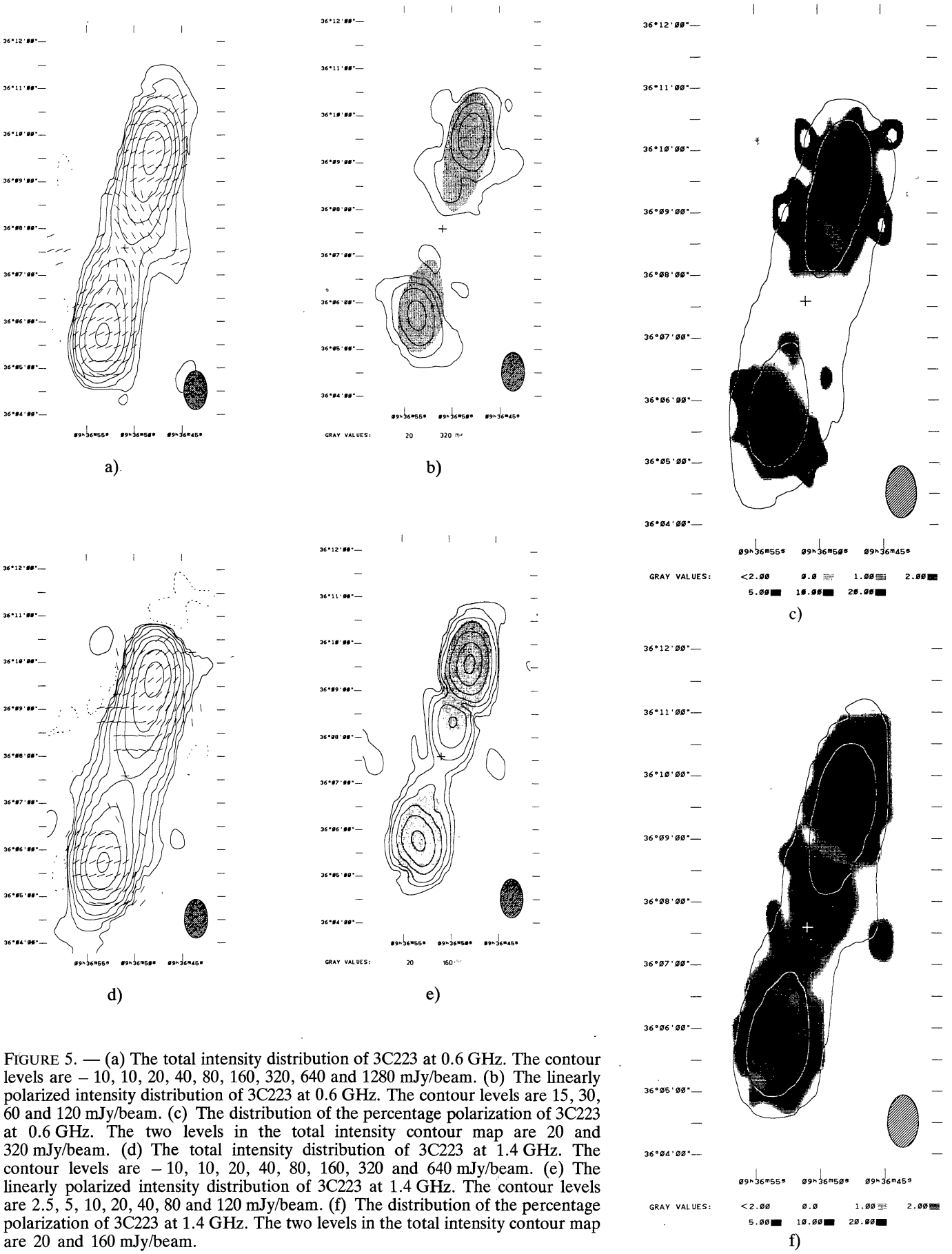

FIGURE 5. — (a) The total intensity distribution of 3C223 at 0.6 GHz. The contour levels are – 10, 10, 20, 40, 80, 160, 320, 640 and 1280 mJy/beam. (b) The linearly polarized intensity distribution of 3C223 at 0.6 GHz. The contour levels are 15, 30, 60 and 120 mJy/beam. (c) The distribution of the percentage polarization of 3C223 at 0.6 GHz. The two levels in the total intensity contour map are 20 and 320 mJy/beam. (d) The total intensity distribution of 3C223 at 1.4 GHz. The contour levels are – 10, 10, 20, 40, 80, 160, 320 and 640 mJy/beam. (e) The linearly polarized intensity distribution of 3C223 at 1.4 GHz. The contour levels are 2.5, 5, 10, 20, 40, 80 and 120 mJy/beam. (f) The distribution of the percentage polarization of 3C223 at 1.4 GHz. The two levels in the total intensity contour map are 20 and 160 mJy/beam.

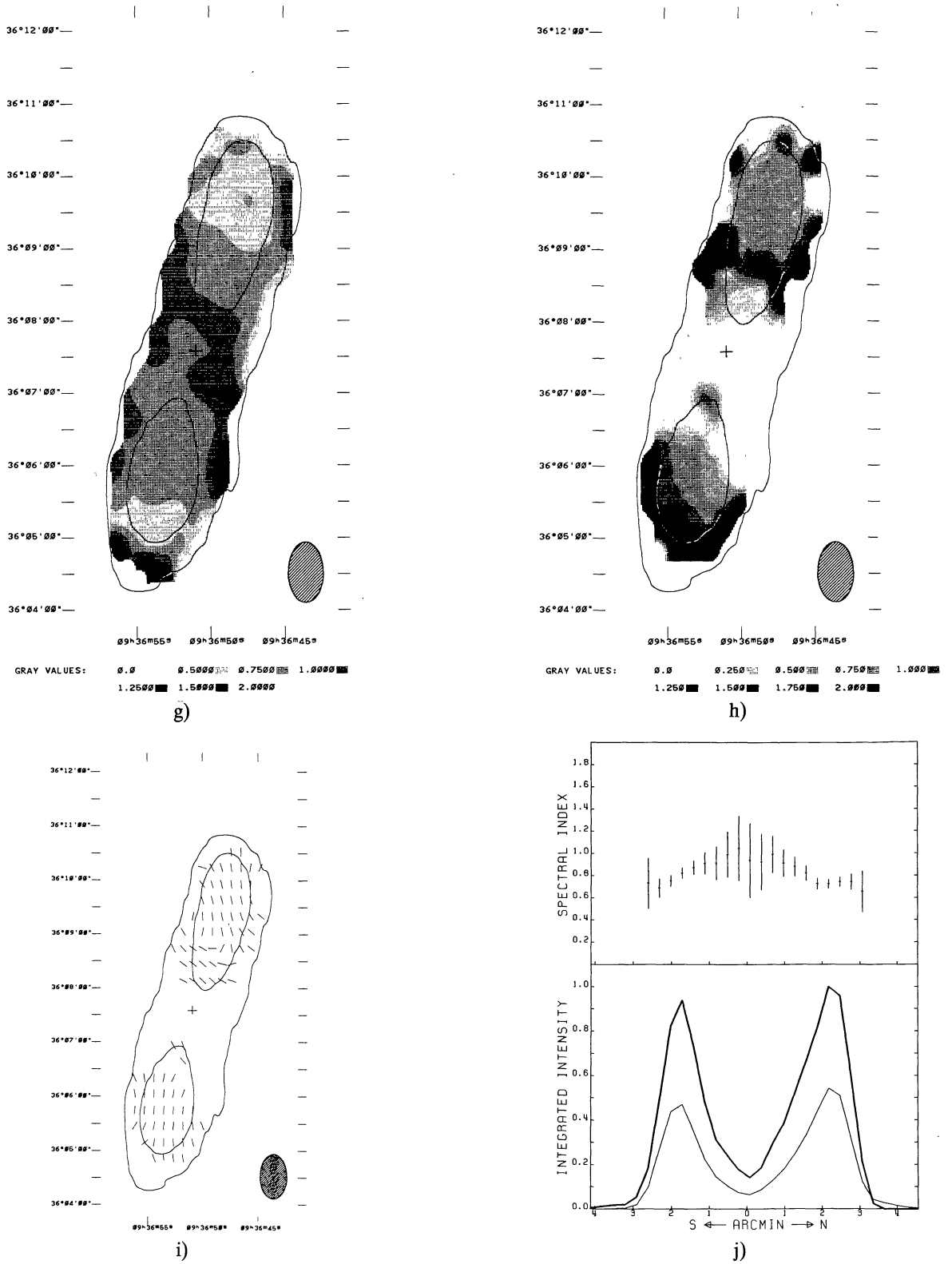

FIGURE 5. — (g) The distribution of the spectral index of 3C223 between 0.6 GHz and 1.4 GHz. The two levels in the total intensity contour map at 0.6 GHz are 20 and 320 mJy/beam. (h) The distribution of the depolarization of 3C223 between 0.6 GHz and 1.4 GHz the two levels in the total intensity contour map at 0.6 GHz are 20 and 320 mJy/beam. (i) The distribution of the rotation of the polarization position angle of 3C223 between 0.6 GHz and 1.4 GHz measured from the North towards the East. The two levels in the total intensity contour map at 0.6 GHz are 20 and 320 mJy/beam. (j) The spectral index variations along the major axis of 3C223 between 0.6 GHz and 1.4 GHz. The lower panel shows the (integrated) total intensity along the radio source at 0.6 GHz (thick line) and at 1.4 GHz (thin line). The upper panel shows the variations of the spectral index along the radio source.

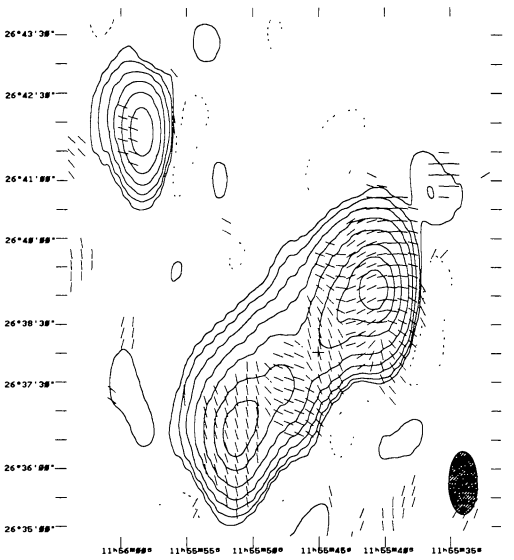

a)

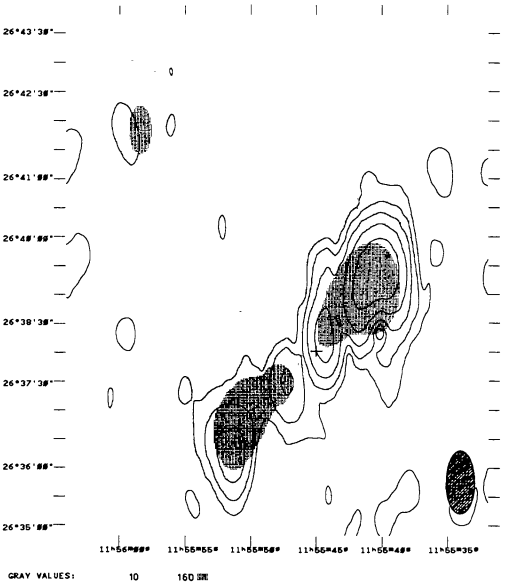

b)

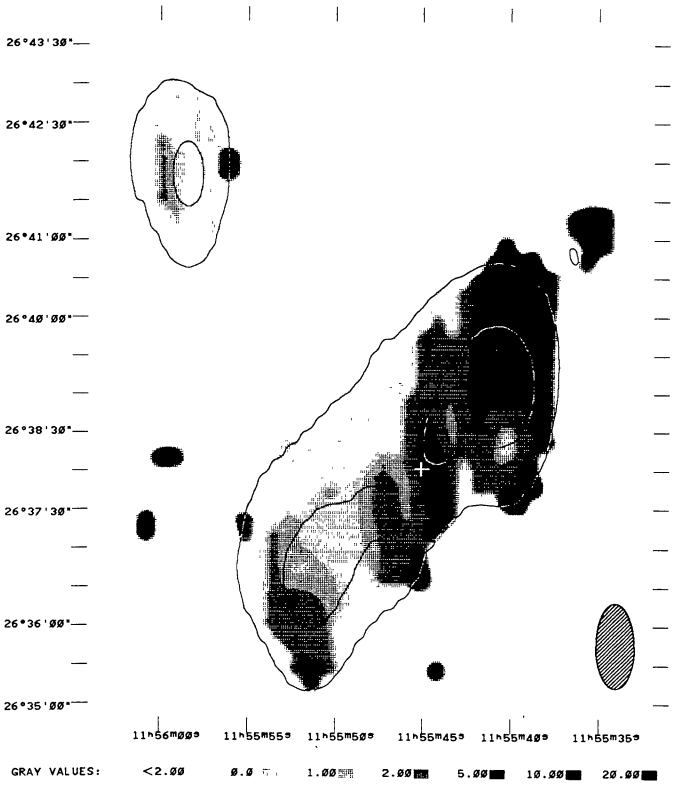

c)

FIGURE 6. — (a) The total intensity distribution of 4C26.35A at 0.6 GHz. The contour levels are – 5, 5, 10, 20, 40, 80, 160, 240 and 320 mJy/beam. (b) The linearly polarized intensity distribution of 4C26.35A at 0.6 GHz. The contour levels are 1, 2, 4, 8 and 16 mJy/beam. (c) The distribution of the percentage polarization of 4C26.35A at 0.6 GHz. The two levels in the total intensity contour map are 10 and 160 mJy/beam.

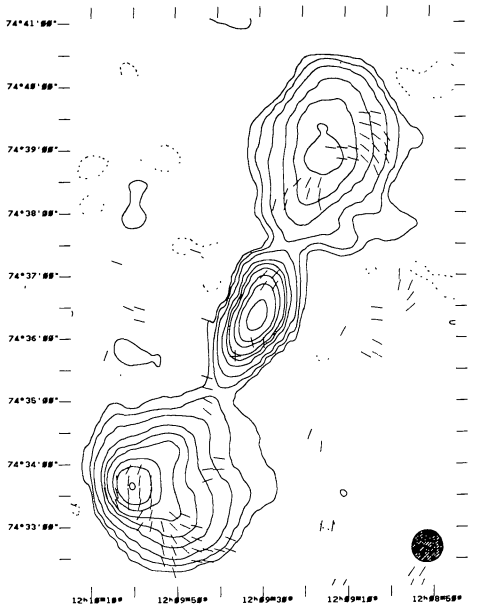

a)

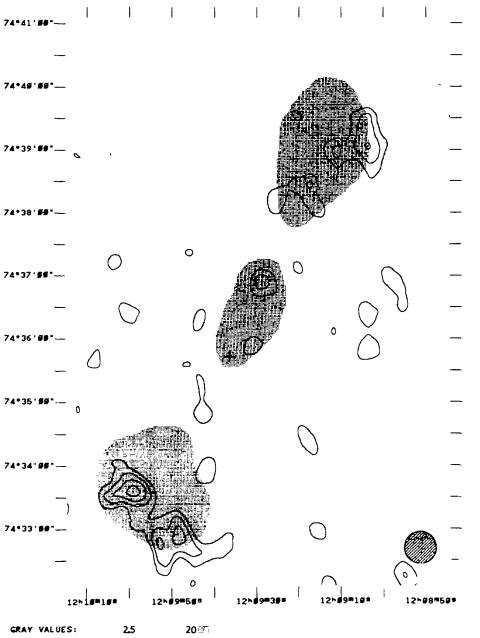

b)

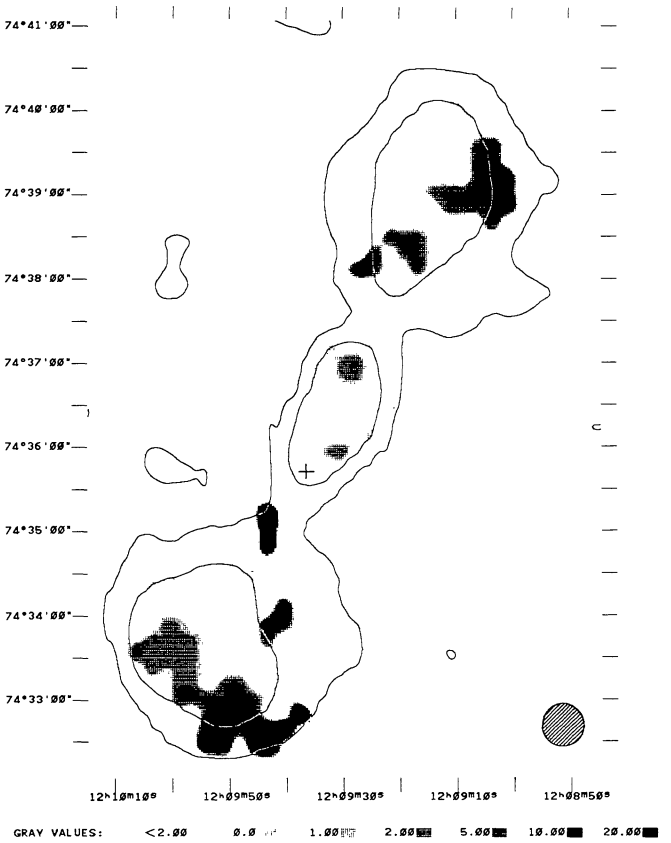

c)

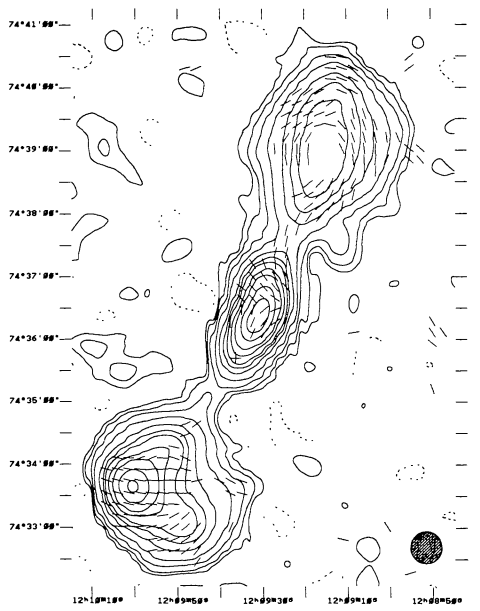

d)

FIGURE 7. — (a) The total intensity distribution of 4C74.17.1 at 0.6 GHz. The contour levels are – 2.5, 2.5, 5, 10, 20, 30, 40, 60, 80 and 120 mJy/beam. (b) The linearly polarized intensity distribution of 4C74.17.1 at 0.6 GHz. The contour levels are 1.5, 2, 2.5 and 3 mJy/beam. (c) The distribution of the percentage polarization of 4C74.17.1 at 0.6 GHz. The two levels in the total intensity contour map are 2.5 and 20 mJy/beam. (d) The total intensity distribution of 4C74.17.1 at 1.4 GHz. The contour levels are – 0.5, 0.5, 1, 2, 4, 8, 12, 16, 24, 32, 48 and 64 mJy/beam.

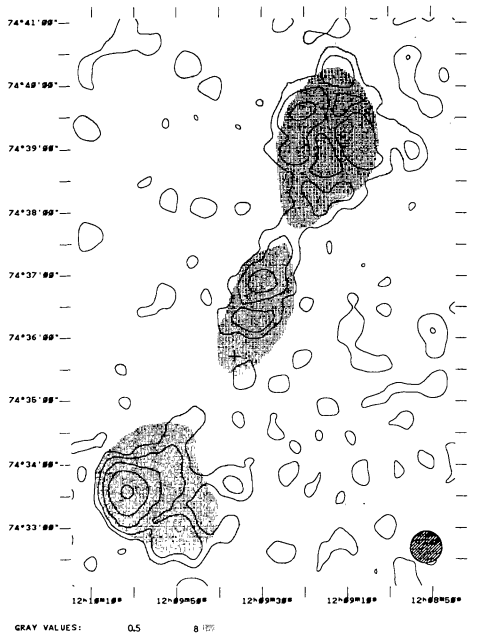

e)

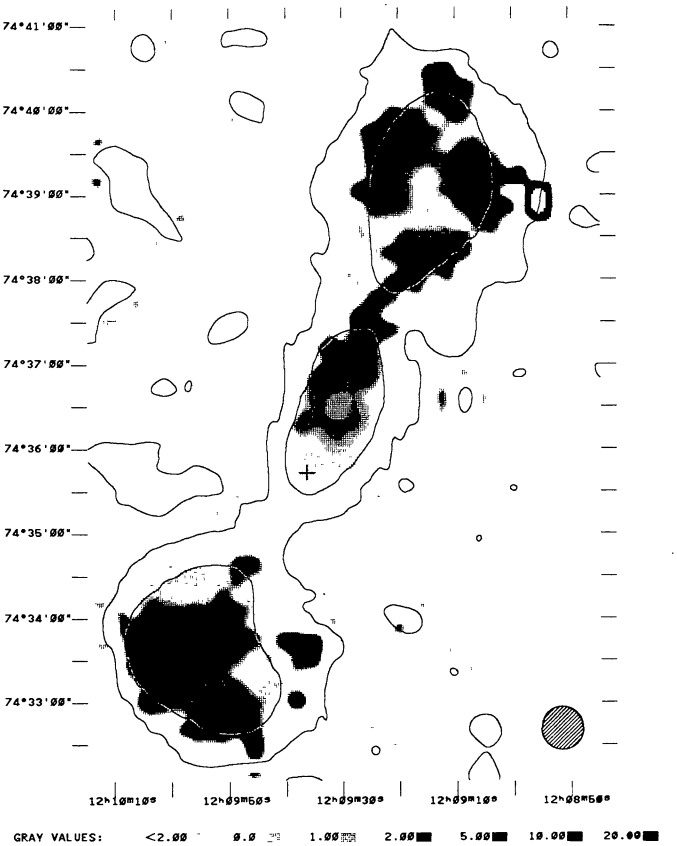

f)

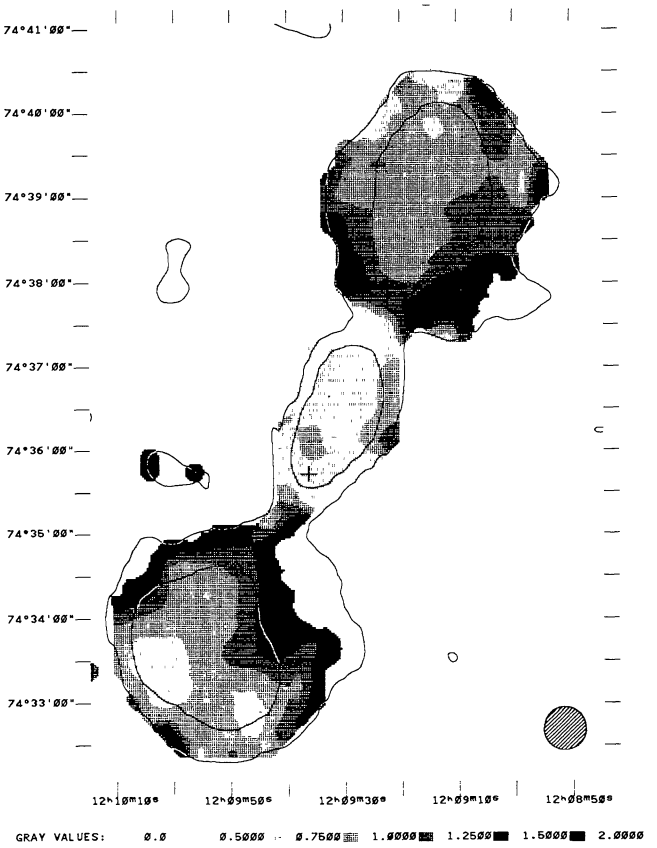

g)

FIGURE 7. — (e) The linearly polarized intensity distribution of 4C74.17.1 at 1.4 GHz. The contour levels are 0.5, 1, 2, 4 and 8 mJy/beam. (f) The distribution of the percentage polarization of 4C74.17.1 at 1.4 GHz. The two levels in the total intensity contour map are 0.5 and 8 mJy/beam. (g) The distribution of the spectral index of 4C74.17.1 between 0.6 GHz and 1.4 GHz. The two levels in the total intensity contour map at 0.6 GHz are 2.5 and 20 mJy/beam.

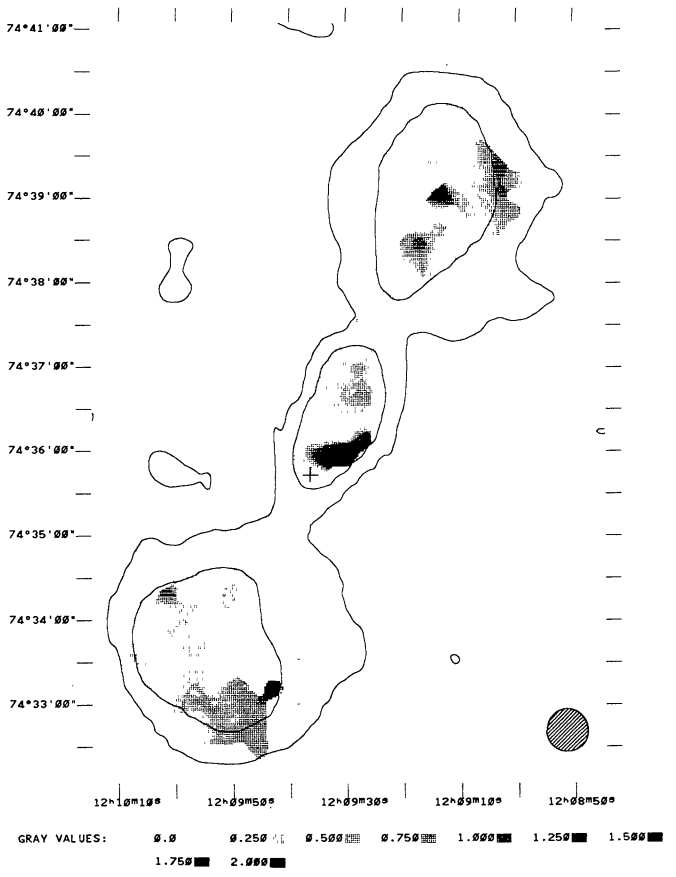

h)

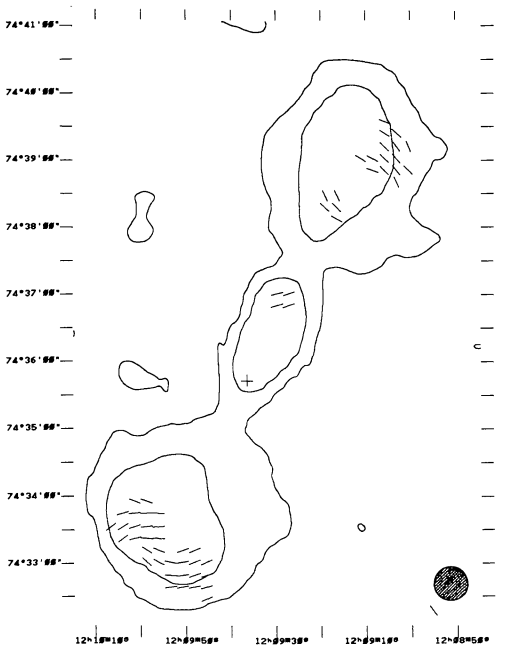

i)

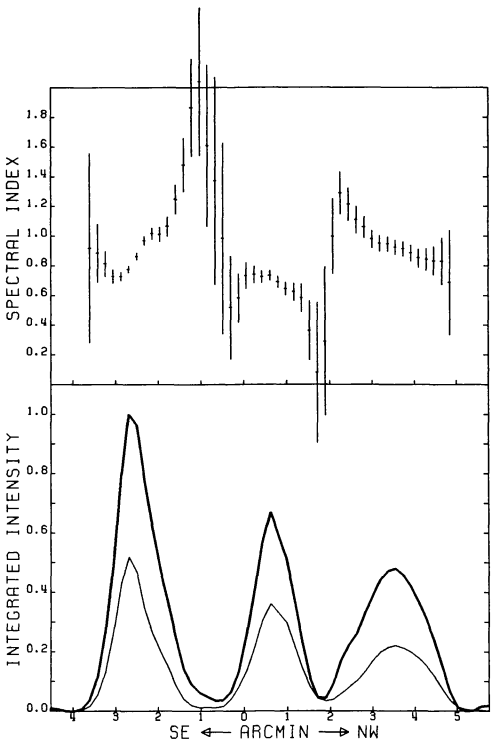

j)

FIGURE 7. — (h) The distribution of the depolarization of 4C74.17.1 between 0.6 GHz and 1.4 GHz. The two levels in the total intensity contour map at 0.6 GHz are 2.5 and 20 mJy/beam. (i) The distribution of the rotation of the polarization position angle of 4C74.17.1 between 0.6 GHz and 1.4 GHz measured from the North towards the East. The two levels in the total intensity contour map at 0.6 GHz are 2.5 and 20 mJy/beam. (j) The spectral index variations along the major axis of 4C74.17.1 between 0.6 GHz and 1.4 GHz. The lower panel shows the (integrated) total intensity along the radio source at 0.6 GHz (thick line) and at 1.4 GHz (thin line). The upper panel shows the variations of the spectral index along the radio source.

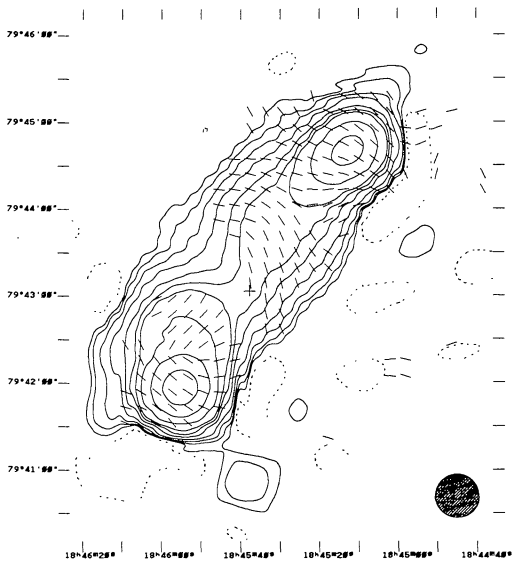

a)

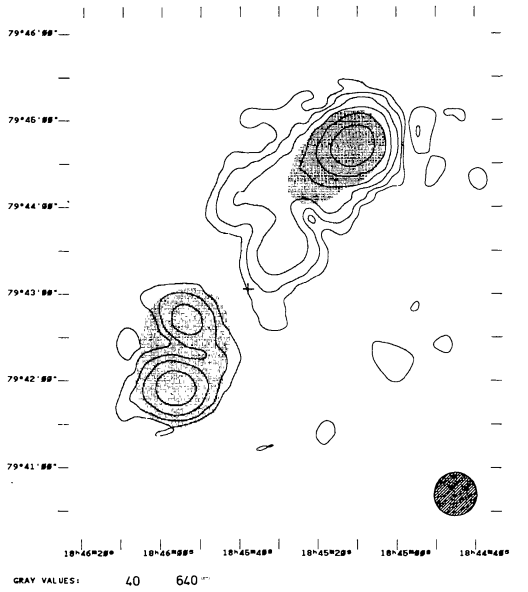

b)

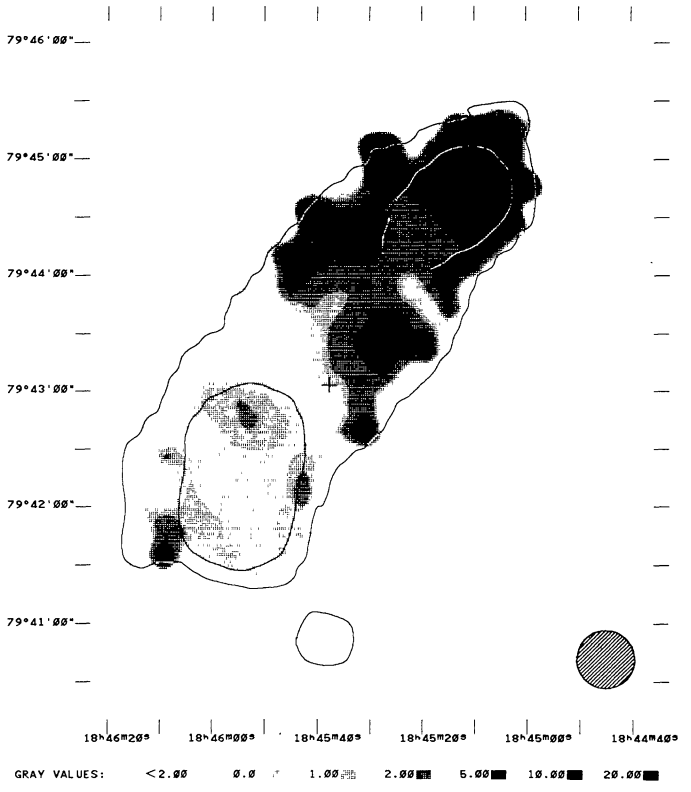

c)

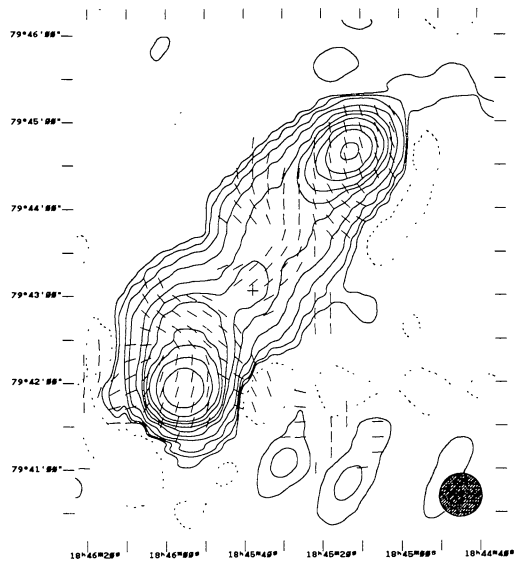

d)

FIGURE 8. — (a) The total intensity distribution of 3C390.3 at 0.6 GHz. The contour levels are – 20, 20, 40, 80, 160, 240, 480, 640, 1280, 2560 and 5120 mJy/beam. (b) The linearly polarized intensity distribution of 3C390.3 at 0.6 GHz. The contour levels are 5, 10, 20, 40, 80 and 160 mJy/beam. (c) The distribution of the percentage polarization of 3C390.3 at 0.6 GHz. The two levels in the total intensity contour map are 40 and 640 mJy/beam. (d) The total intensity distribution of 3C390.3 at 1.4 GHz. The contour levels are – 15, 15, 30, 60, 120, 240, 360, 480, 720, 960, 1440 and 2400 mJy/beam.

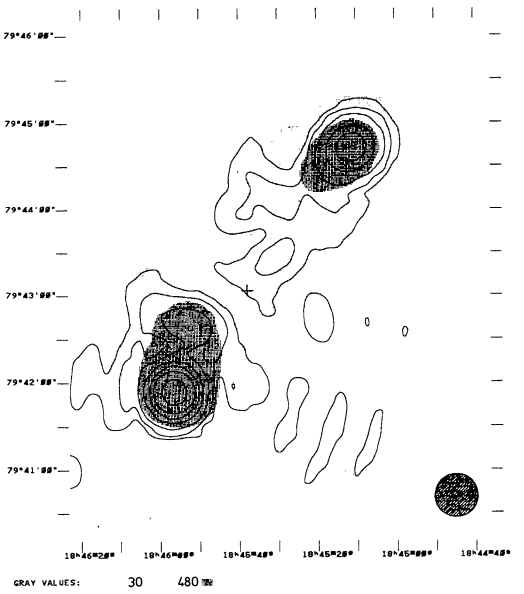

e)

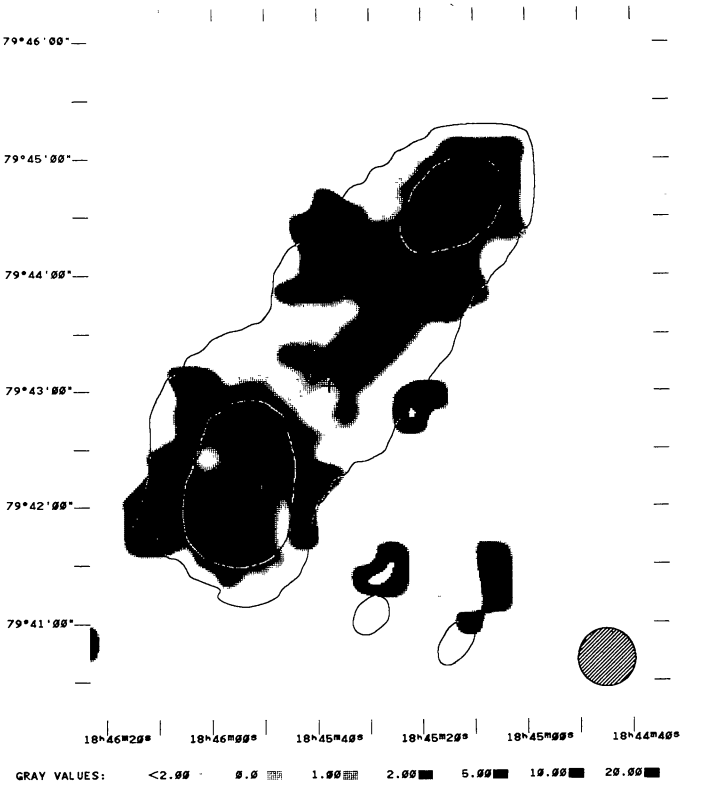

f)

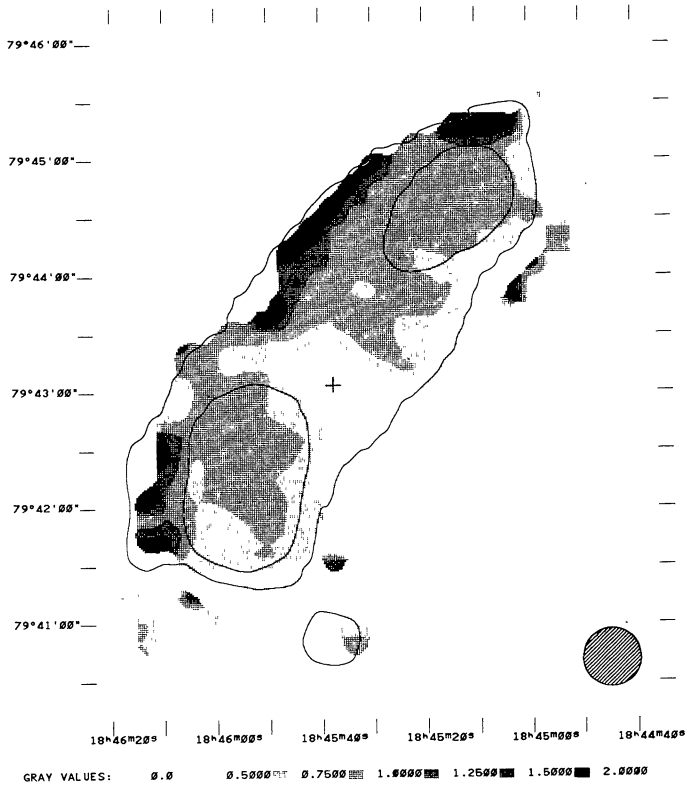

g)

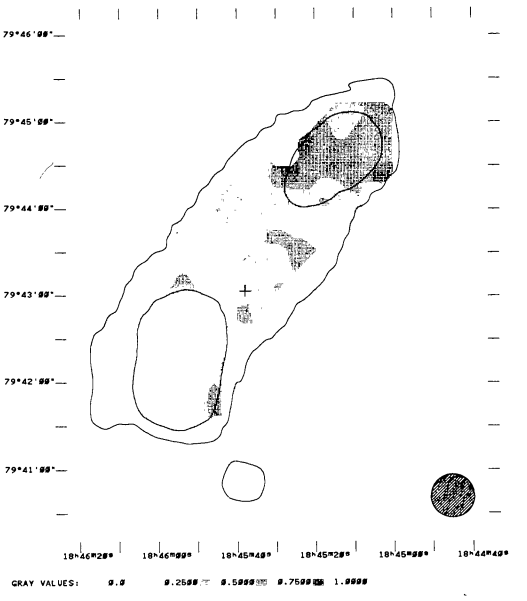

h)

FIGURE 8. — (e) The linearly polarized intensity distribution of 3C390.3 at 1.4 GHz. The contour levels are 15, 30, 60, 120, 180, 240 and 360 mJy/beam. (f) The distribution of the percentage polarization of 3C390.3 at 1.4 GHz. The two levels in the total intensity contour map are 30 and 480 mJy/beam. (g) The distribution of the spectral index of 3C390.3 between 0.6 GHz and 1.4 GHz. The two levels in the total intensity contour map at 0.6 GHz are 40 and 640 mJy/beam. (h) The distribution of the depolarization of 3C390.3 between 0.6 GHz and 1.4 GHz. The two levels in the total intensity contour map at 0.6 GHz are 40 and 640 mJy/beam.

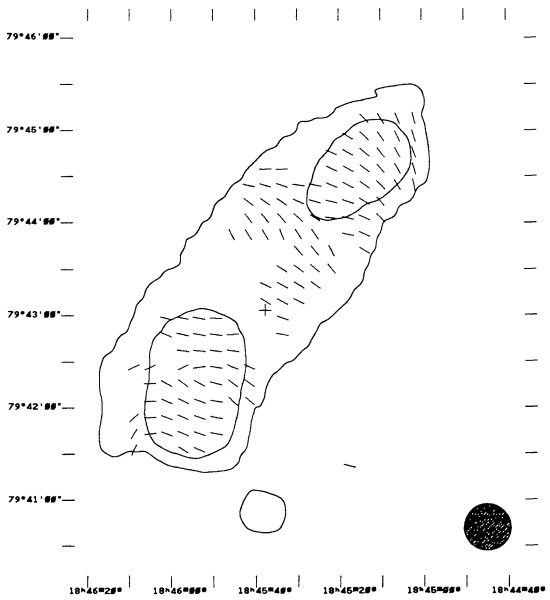

i)

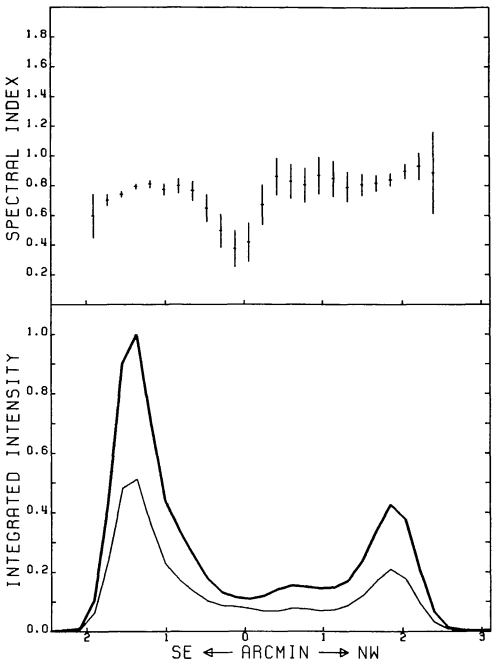

j)

FIGURE 8. — (i) The distribution of the rotation of the polarization position angle of 3C390.3 between 0.6 GHz and 1.4 GHz measured from the North towards the East. The two levels in the total intensity contour map at 0.6 GHz are 40 and 640 mJy/beam. (j) The spectral index variations along the major axis of 3C390.3 between 0.6 GHz and 1.4 GHz. The lower panel shows the (integrated) total intensity along the radio source at 0.6 GHz (thick line) and at 1.4 GHz (thin line). The upper panel shows the variations of the spectral index along the radio source.

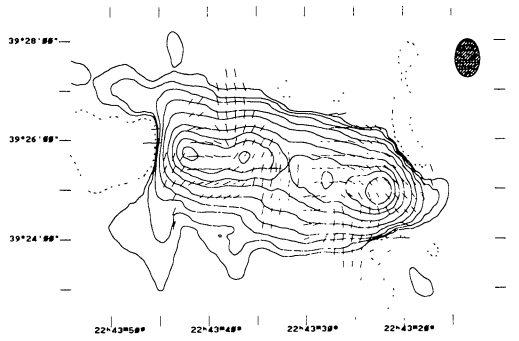

a)

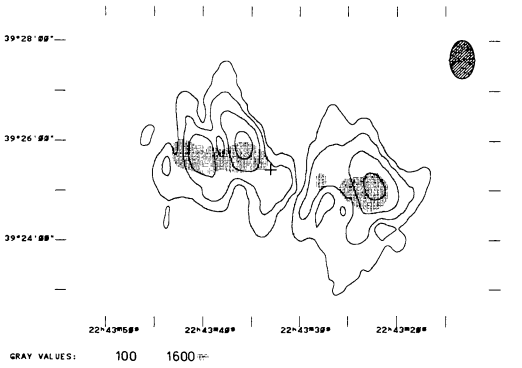

b)

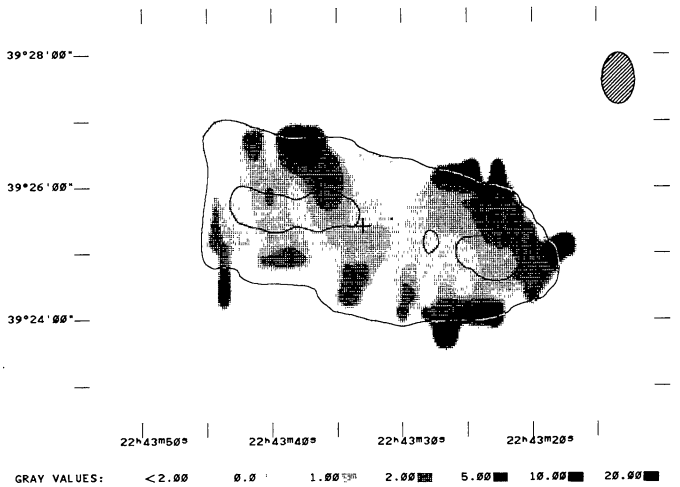

c)

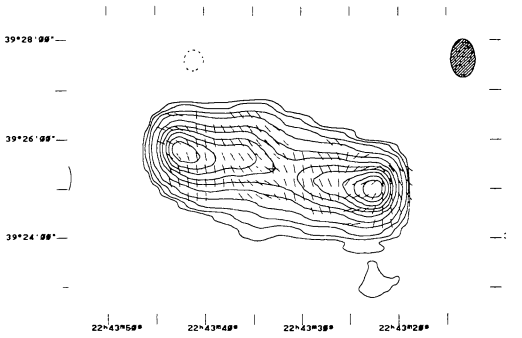

d)

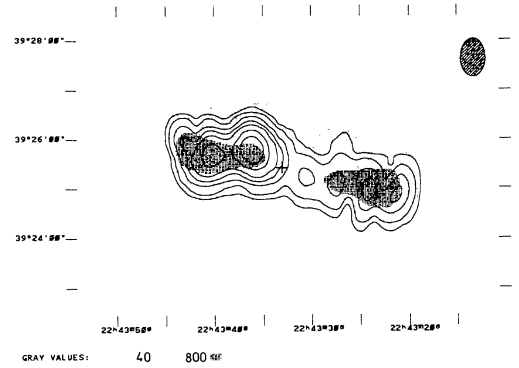

e)

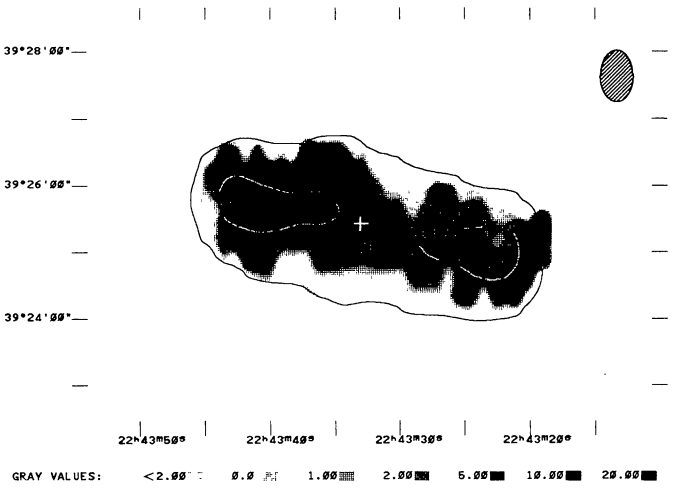

f)

FIGURE 9. — (a) The total intensity distribution of 3C452 at 0.6 GHz. The contour levels are – 25, 25, 50, 100, 200, 400, 800, 1200 and 2000 mJy/beam. (b) The linearly polarized intensity distribution of 3C452 at 0.6 GHz. The contour levels are 5, 10, 20 and 40 mJy/beam. (c) The distribution of the percentage polarization of 3C452 at 0.6 GHz. The two levels in the total intensity contour map are 100 and 1600 mJy/beam. (d) The total intensity distribution of 3C452 at 1.4 GHz. The contour levels are – 20, 20, 40, 80, 160, 320, 480, 640, 800, 960, 1120 and 1280 mJy/beam. (e) The linearly polarized intensity distribution of 3C452 at 1.4 GHz. The contour levels are 10, 20, 40, 60, 80, 120 and 160 mJy/beam. (f) The distribution of the percentage polarization of 3C452 at 1.4 GHz. The two levels in the total intensity contour map are 40 and 800 mJy/beam.

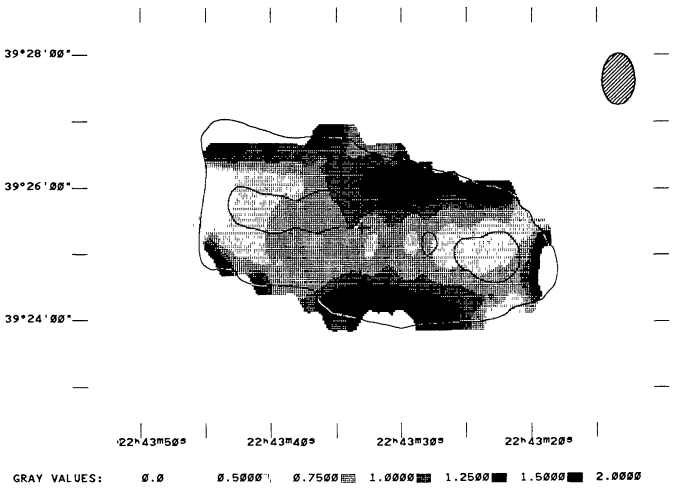

g)

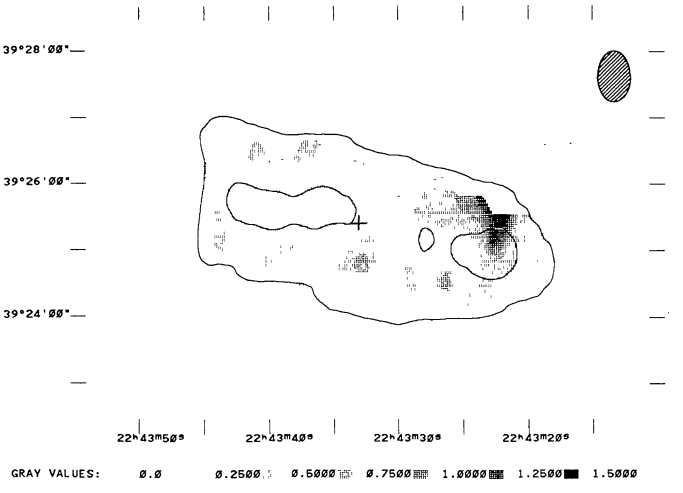

h)

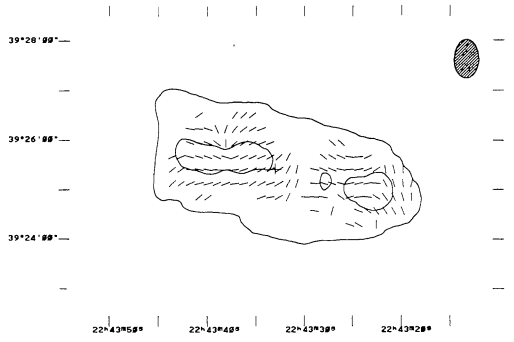

i)

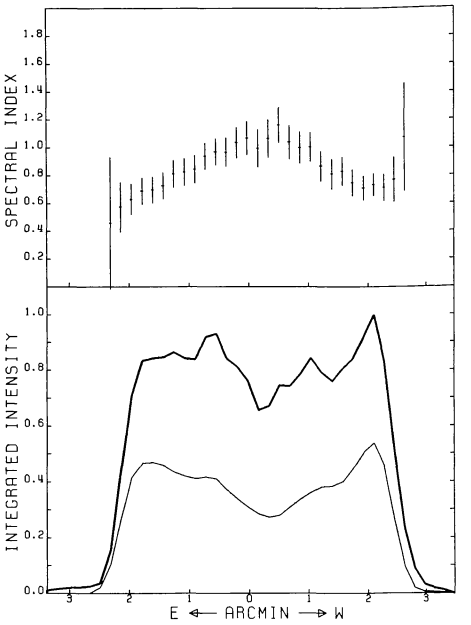

j)

FIGURE 9. — (g) The distribution of the spectral index of 3C452 between 0.6 GHz and 1.4 GHz. The two levels in the total intensity contour map at 0.6 GHz are 100 and 1600 mJy/beam. (h) The distribution of the depolarization of 3C452 between 0.6 GHz and 1.4 Ghz. The two levels in the total intensity contour map at 0.6 Ghz are 100 and 1600 mJy/beam. (i) The distribution of the rotation of the polarization position angle of 3C452 between 0.6 GHz and 1.4 GHz measured from the North towards the East. The two levels in the total intensity contour map at 0.6 GHz are 100 and 1600 mJy/beam. (j) The spectral index variations along the major axis of 3C452 between 0.6 GHz and 1.4 GHz. The lower panel shows the (integrated) total intensity along the radio source at 0.6 GHz (thick line) and at 1.4 GHz (thin line). The upper panel shows the variations of the spectral index along the radio source.